




Adaptation to high rates of chromosomal instability and aneuploidy through multiple pathways in budding yeast

Matthew N Clarke , Theodor Marsoner , Manuel Alonso Y Adell, Madhwesh C Ravichandran & Christopher S Campbell* 

Abstract

Both an increased frequency of chromosome missegregation (chromosomal instability, CIN) and the presence of an abnormal complement of chromosomes (aneuploidy) are hallmarks of cancer. To better understand how cells are able to adapt to high levels of chromosomal instability, we previously examined yeast cells that were deleted of the gene *BIR1*, a member of the chromosomal passenger complex (CPC). We found *bir1Δ* cells quickly adapted by acquiring specific combinations of beneficial aneuploidies. In this study, we monitored these yeast strains for longer periods of time to determine how cells adapt to high levels of both CIN and aneuploidy in the long term. We identify suppressor mutations that mitigate the chromosome missegregation phenotype. The mutated proteins fall into four main categories: outer kinetochore subunits, the SCF^{Cdc4} ubiquitin ligase complex, the mitotic kinase Mps1, and the CPC itself. The identified suppressor mutations functioned by reducing chromosomal instability rather than alleviating the negative effects of aneuploidy. Following the accumulation of suppressor point mutations, the number of beneficial aneuploidies decreased. These experiments demonstrate a time line of adaptation to high rates of CIN.

Keywords aneuploidy; Aurora B; chromosomal instability; kinetochore; SCF complex

Subject Categories Cell Cycle; DNA Replication, Recombination & Repair

DOI 10.15252/emboj.2022111500 | Received 22 April 2022 | Revised 8 November 2022 | Accepted 24 November 2022 | Published online 19 December 2022

The EMBO Journal (2023) 42: e111500

See also: [Z Storchová](#) (April 2023)

Introduction

The accurate distribution of chromosomes to daughter cells is a fundamental requirement of cell division. An increase in the frequency of errors in chromosome segregation is called chromosomal instability (CIN). Chromosomal instability leads to abnormal karyotypes through the gain or loss of chromosomes, a state called aneuploidy.

Aneuploidy and CIN are both hallmarks of cancer that have causative roles in cancer development, cancer progression, and resistance to chemotherapy (reviewed in Ben-David & Amon, 2020). Despite the promotion of cell proliferation in cancer, aneuploidy and CIN have consistently been demonstrated to decrease cell growth and division (Gropp *et al*, 1983; Torres *et al*, 2007). Cancers therefore likely develop adaptations to ameliorate the negative effects of CIN and aneuploidy.

Different models for how cells adapt to CIN and aneuploidy have been proposed. Cells could adapt via compensatory mutations that decrease the levels of CIN after the accumulation of beneficial aneuploidies (Cahill *et al*, 1999; Kwon *et al*, 2008; Sansregret *et al*, 2017). Alternatively, researchers postulated that cancer cells could adapt to CIN and aneuploidy through mutations that lead to aneuploidy tolerance (Torres *et al*, 2010). Additionally, it was suggested that CIN and aneuploidy provide for a fast, but transient mechanism of adaptation. In this model, aneuploidy provides a short-term benefit that outweighs its downsides but would eventually be superseded by more targeted genome alterations (Yona *et al*, 2012). How aneuploidy and more specific types of mutations affect each other during the course of adaptation is currently unknown.

The molecular mechanisms that lead to CIN in cancer cells have long been elusive (Gordon *et al*, 2012). However, one relevant phenotype that is frequently observed across many cancer types is the overstabilization of connections between microtubules and kinetochores, which are the binding sites for microtubules at the centromeres of chromosomes (Bakhoum *et al*, 2009a). These overstabilized attachments lead to the accumulation of misattached chromosomes where both of the sister chromatids are attached to microtubules emanating from the same spindle pole (merotelic and syntelic attachments). One or both of the kinetochores must then be detached from the microtubules in order to properly distribute one sister chromatid to each daughter cell. Although the basis behind this phenotype in cancer cells is currently unknown, the central player in destabilizing erroneous kinetochore–microtubule attachments is the chromosomal passenger complex (CPC). The CPC contains a kinase, Aurora B, that phosphorylates kinetochores to lower their affinity for microtubules (Tanaka *et al*, 2002; Cheeseman *et al*,

2006; Sarangapani *et al*, 2013; Kalantzaki *et al*, 2015). Inhibition of Aurora B in mammalian cells leads to an increased frequency of lagging chromosomes in anaphase due to the inability to detach microtubules from kinetochores that are attached to both spindle poles (Cimini *et al*, 2006). This lagging chromosome phenotype is also frequently observed in cancers (Bakhoun *et al*, 2014).

In addition to Aurora B, the CPC contains the subunits INCENP, Survivin, and Borealin. The C-terminus of INCENP binds to and activates Aurora B, while the N-terminus binds to Survivin and Borealin (Ainsztein *et al*, 1998; Bishop & Schumacher, 2002; Honda *et al*, 2003; Sessa *et al*, 2005; Klein *et al*, 2006; Jeyaprakash *et al*, 2007). Survivin and Borealin target the complex to centromere-proximal chromatin through an interaction with Shugoshin. This interaction was shown to promote the activity of the CPC in correcting erroneous kinetochore–microtubule attachments through phosphorylation of substrates at the outer kinetochore (Gassmann *et al*, 2004; Kawashima *et al*, 2007, 2010; Vanoosthuyse *et al*, 2007).

The budding yeast *Saccharomyces cerevisiae* is a valuable model organism for studying CIN and aneuploidy as it can tolerate high levels of CIN that are similar to what is frequently observed in cancer. We previously determined how cells initially adapt to extremely high rates of chromosome missegregation by growing budding yeast cells carrying mutations that decrease CPC function (Ravichandran *et al*, 2018). The budding yeast homologs of the CPC subunits Aurora B, INCENP, Survivin, and Borealin are Ipl1, Sli15, Bir1, and Nbl1, respectively (Fig 1A). By sequencing populations of yeast that were grown in the absence of the CPC subunit Survivin/Bir1, we found that the yeast adapted by acquiring specific aneuploidies that decreased the rate of CIN (Ravichandran *et al*, 2018). The compositions of karyotypes were further refined over time until the cells acquired certain combinations of beneficial aneuploid chromosomes. However, these adapted cells were still substantially less fit than wild-type due to a combination of the negative effects of the acquired aneuploidies and residual chromosomal instability. It is currently not known how cells with high rates of CIN and aneuploidy further adapt after the initial optimization of their karyotypes.

In this study, we have now monitored these CPC-deficient cells for longer periods of time to determine how cells evolve to cope in the long term with increased levels of both CIN and aneuploidy. We aimed to determine whether they adapt through genetic changes that either (i) allow for better aneuploidy tolerance, (ii) decrease the levels of CIN, or (iii) further optimize their karyotypes. We found

that cells evolved through hypomorphic mutations in essential genes that decreased the levels of CIN. The lower levels of CIN then allowed the cells to decrease their levels of aneuploidy, as the beneficial effects of the extra chromosomes no longer outweighed the fitness costs. The identified mutations fall into two broad functional categories. The first category of mutations destabilizes kinetochore–microtubule interactions, counteracting the overstabilization created by decreased CPC activity. These mutations were found in outer kinetochore proteins that directly interact with microtubules. The second category of mutations affect the function of the CPC more directly. These include mutations in the CPC itself, the mitotic kinase Mps1, and the ubiquitin ligase SCF^{Cdc4} complex. SCF^{Cdc4} mutations increase the recruitment of the CPC to key regulatory regions in both yeast and human cells. We conclude that cells generally adapt to high levels of CIN and aneuploidy through mutations that alleviate the CIN phenotype. Furthermore, we have identified specific pathways of adaptation to defects in CPC function.

Results

Adaptation to high levels of CIN and aneuploidy occurs through point mutations that reduce the rate of CIN

To determine how cells adapt to high rates of CIN and aneuploidy, we started with a collection of haploid yeast strains that were previously cultured for 21 days via clonal expansion following *BIR1* deletion (Ravichandran *et al*, 2018). We call these partially adapted strains *bir1Δ-ad*. These strains have a high frequency of specific aneuploidies that decrease the rate of CIN. However, they are not enriched for mutations that are related to CIN. We adapted 68 of these strains for an additional 21 or 42 days (*bir1Δ-ad2*) in liquid culture to determine how cells continue to evolve after their initial adaptation through aneuploidy (Fig 1B). In comparison with the clonal expansion of the initial adaptation, liquid culture adaptation allows time for rarely occurring beneficial genomic changes to take over the population competitively. This additional adaptation greatly improved the growth of some strains but did not result in a significant level of growth improvement for all of the adapted populations combined (Fig 1C). Cells with impaired chromosome segregation are especially sensitive to microtubule-depolymerizing drugs. Consistent with this, *BIR1* deletion results in a strong sensitivity to moderate amounts of the microtubule-depolymerizing drug benomyl

Figure 1. Strains with high levels of CIN and aneuploidy adapt by decreasing CIN.

- A Schematic summarizing the main localization of the CPC and its role in phosphorylating the Dam1 complex (Dam1c) to destabilize microtubule attachments.
- B Summary of the adaptation time-line. *bir1Δ* strains from tetrads were grown clonally for 21 days to produce *bir1Δ-ad* strains. Colonies from the *bir1Δ-ad* strains were then grown in liquid media for 21 or 42 additional days to produce the *bir1Δ-ad2* strains.
- C, D Growth comparisons of wild-type (WT, *n* = 16), unadapted (*bir1Δ*, *n* = 14), partially adapted (*bir1Δ-ad*, *n* = 15), and further adapted (*bir1Δ-ad2*, *n* = 15) strains as measured by area of growth after serial dilution. The serial dilutions of all these strains were carried out once in parallel. Examples of dilutions series such as those used in the quantification for *bir1Δ-ad* and *bir1Δ-ad2* strains can be found in Fig EV1C. Ten-fold serial dilutions were made on YPAD plates containing either 0.1% DMSO (C) or 10 μg/ml of benomyl (D). The mean (red line) is shown. Growth was normalized to WT.
- E Comparison of the mean number of aneuploid chromosomes per strain for the *bir1Δ-ad* (*n* = 45 strains) and *bir1Δ-ad2* (*n* = 51 strains) collections. Only data from *bir1Δ-ad* strains that were subjected to additional adaptation are shown. Means and standard deviations are shown.
- F Histogram showing the proportion of strains that are aneuploid for specific chromosomes in partially adapted (*bir1Δ-ad*) and further adapted (*bir1Δ-ad2*) strains.
- G Eight hundred and seventy-four genes out of 6,002 total yeast genes (14.5%) have phenotypes related to CIN. The percentage of newly identified mutations in the *bir1Δ-ad2* (26 out of 98) and *bir1Δ-ad* (37 out of 246) strains that are related to CIN are shown.

Data information: (ns) not significant; (*) *P* < 0.05; unpaired t-test.

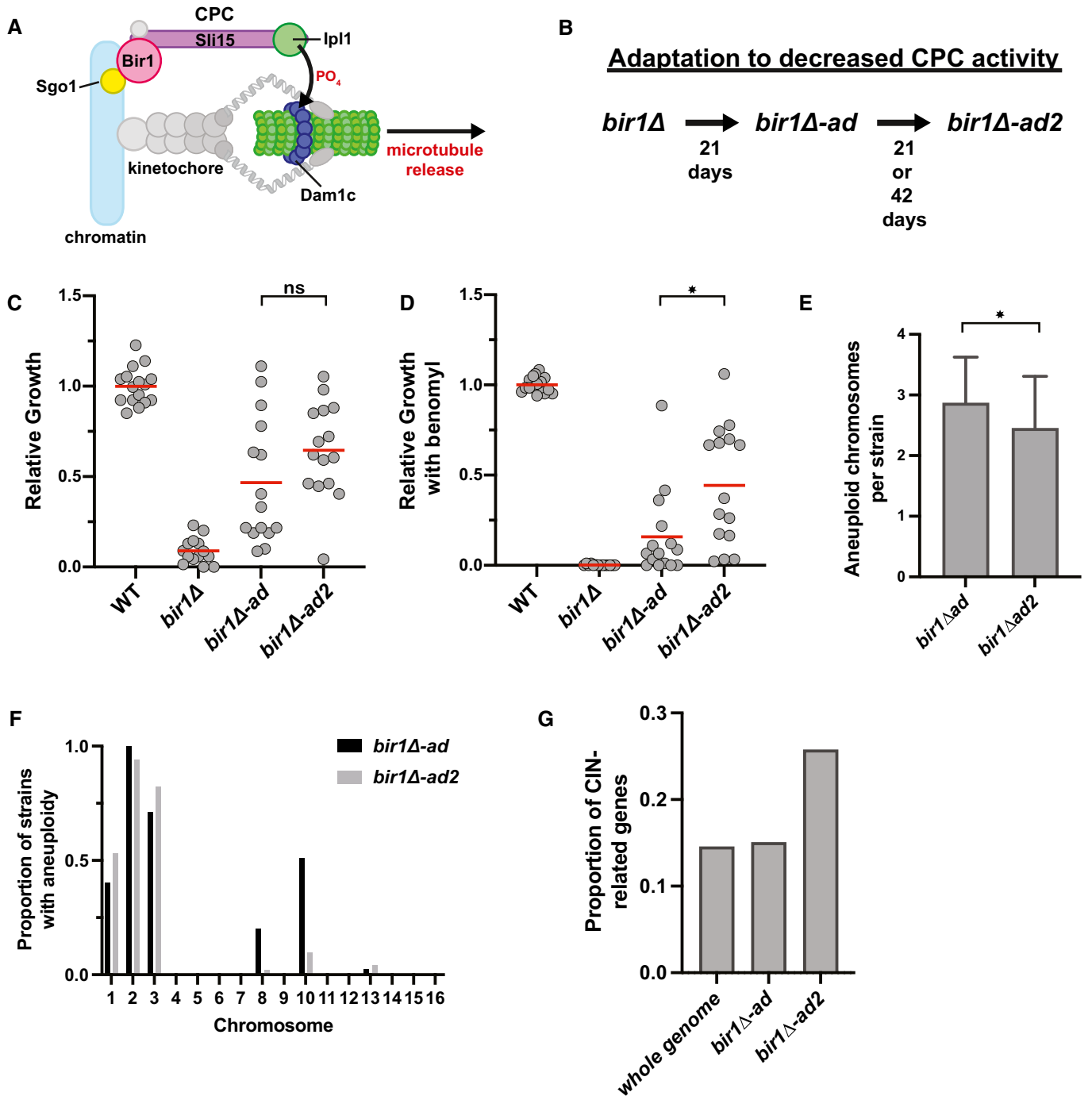


Figure 1.

(Makrantonis & Stark, 2009). Many of the *bir1Δ-ad2* strains have strongly decreased benomyl sensitivity in comparison with the *bir1Δ-ad* strains, suggesting that they have acquired additional changes that suppress the CIN phenotype (Fig 1D). To determine whether this additional adaptation occurs through further increased aneuploidy, we measured chromosome copy numbers via read counts from whole-genome sequencing. Two strains that were observed to have large segmental amplifications of chromosomes 2 and 13 were excluded from this analysis. Overall, the *bir1Δ-ad2*

strains have decreased numbers of aneuploid chromosomes, suggesting that these strains do not adapt through further increases in aneuploid chromosomes that attenuate CIN (Fig 1E and F). We conclude that the additional adaptation to CIN in the further adapted CPC-deficient strains likely comes from specific mutations rather than chromosome copy number alterations.

Adaptation to CIN and aneuploidy could potentially come from mutations that either decrease CIN or increase aneuploidy tolerance. To determine whether mutations in the adapted strains fall into

these categories, we searched for nonsynonymous mutations that arose during liquid culture adaptation in the whole-genome sequencing data. We identified 97 such mutations in 68 strains. These mutations were enriched in genes related to CIN (Fig 1G). Mutations that increase aneuploidy tolerance were previously reported in budding yeast (Torres *et al*, 2010). However, there was no overlap between the 22 genes identified in the aneuploidy tolerance screen and the genes mutated in the *bir1Δ-ad2* strains. We therefore used the most heavily characterized gene whose loss leads to aneuploidy tolerance, the ubiquitin-specific protease *UBP6* (Torres *et al*, 2010). We tested whether a mutation in *UBP6* that was previously reported to increase aneuploidy tolerance would increase resistance to *bir1Δ*. The mutation was introduced into a haploid strain whose only copy of *BIR1* is on a minichromosome that also contains the *URA3* gene. This minichromosome can be selected against using 5-Fluoroorotic acid (5-FOA), which is converted into a toxin by the *URA3* gene product. The addition of the *ubp6(E256X)* mutation did not increase viability after *BIR1* was deleted (Fig EV1A). This result suggests that aneuploidy tolerance does not lead to CIN tolerance following *BIR1* deletion. We note that we used the same strain background as the studies that identified and

characterized the role of *UBP6* in tolerating aneuploidy (W303), which has been shown to have a mutation in the *SSD1* gene that makes them more sensitive to aneuploidy (Hose *et al*, 2020). We conclude that cells with high levels of CIN and aneuploidy adapt primarily through mutations that mitigate CIN rather than aneuploidy.

bir1Δ suppressor mutations fall into four major categories

To determine which categories of mutations are most prevalent in our adapted strains, we searched for the enrichment of functional gene ontology (GO) terms. We found significant enrichment of genes related to “chromosome segregation” (FDR = 3.53×10^{-5}) and “SCF-dependent proteasomal ubiquitin-dependent protein catabolic process” (FDR = 1.3×10^{-1} , Table EV2). Further refinement of these categories revealed that the mutations fall largely into four categories (Table 1).

The first category is in proteins that form the outer kinetochore, including mutations in the Dam1 complex, the Ndc80 complex, and Spc105/KNL1. All three of these proteins/protein complexes directly bind to microtubules. The Dam1 complex was the most heavily represented in the data set with mutations in five of the 10 subunits.

Table 1. Candidate mutations identified in *bir1Δ-ad2*.

Gene mutated	Residue changes	Tested	Chromosome	Days of liquid adaptation	Essential	Basic function
<i>DUO1</i>	P17L	Yes	7	21	Yes	Kinetochore–microtubule attachment
<i>DAD1</i>	N43S	Yes	4	21	Yes	
<i>DAD2</i>	K11Q	Yes	11	21	Yes	
<i>ASK1</i>	S216F	Yes	11	21	Yes	
<i>SPC34</i>	D119A	Yes	11	21	Yes	
<i>NDC80</i>	K181N	Yes	9	42	Yes	
<i>SPC105</i>	R583G ^a	Yes	7	21	Yes	CPC subunit
<i>SLI15</i>	L71S	Yes	2 ^b	21	Yes	
<i>SLI15</i>	P109A	No	2 ^b	21	Yes	
<i>SLI15</i>	G334S	Yes	2 ^b	21	Yes	S-phase entry
<i>CDC53</i>	K448E	No	4	21	Yes	
<i>CDC53</i>	A486P	No	4	21	Yes	
<i>CDC34</i>	M64T ^a	Yes	4	21	Yes	
<i>CDC4</i>	S438G	Yes	6	21	Yes	
<i>CDC4</i>	G439S	Yes	6	21	Yes	
<i>CDC4</i>	G652D	No	6	21	Yes	Initiation of SAC
<i>MPS1</i>	R596H	Yes	4	21	Yes	
<i>MPS1</i>	W629S	No	4	21	Yes	
<i>MPS1</i>	V631M	Yes	4	21	Yes	Inner kinetochore
<i>MIF2</i>	D241N	Yes	11	42	Yes	
<i>RTG2</i>	G154S	Yes	7	21	Yes	
<i>RTG2</i>	H425L	No	7	21	Yes	Mitochondrial sensor
<i>RTG2</i>	A433P	No	7	21	Yes	
<i>SPC97</i>	S816X	Yes	8 ^b	21	Yes	Spindle pole body

^aIdentified in the same strain.

^bChromosomes that are commonly aneuploid in *bir1Δ* strains.

Mutations in the Dam1 complex subunit Dam1 that mimic Ipl1 phosphorylation were previously shown to suppress CPC mutations (Cheeseman et al, 2002). However, none of the mutations identified in the *bir1Δ-ad2* strains were in the Dam1 protein itself, indicating that they do not directly mimic similar phosphorylation events (Fig 2A). The mutation of lysine 181 in the Ndc80 complex resides in the microtubule binding CHD domain and is similar to the lysine 146 mutation in human Ndc80 that was previously shown to reduce microtubule binding (Ciferri et al, 2008).

The second category of mutations are in the CPC subunit Sli15. Mutations in Sli15 that disrupt binding to Bir1 or prevent Cdc28 (cyclin-dependent kinase) phosphorylation were both previously shown to suppress *BIR1* deletion (Campbell & Desai, 2013). All three of the observed mutations are consistent with these previous observations, as two were in the CEN box that interacts with Bir1 (L71S and P109H) and one was directly adjacent to the main Cdc28 phosphorylation site (G334S).

The third category of common mutations in the adapted strains is in subunits of the SCF ubiquitin-protein ligase complex. The SCF is primarily involved in the initiation of S-phase, but it also has roles in mitosis (Goh & Surana, 1999). We identified mutations in the core SCF subunits Cdc53 and Cdc34 as well as the F-box adaptor protein Cdc4. F-box proteins dictate the substrate specificity of the SCF complex (Jonkers & Rep, 2009). Important substrates of SCF^{Cdc4} include the cell cycle kinase inhibitors Sic1 and Far1. No mutations in any other F-box proteins were identified, suggesting that the ability to suppress *BIR1* deletion may be specific to SCF^{Cdc4}. All three Cdc4 mutations were in the WD-40 domain, which directly interacts with SCF complex substrates (Fig 2A). No direct connection between the SCF complex and the CPC has been previously identified.

The final category of potential suppressor mutations was in the mitotic kinase Mps1. All three of the mutations in Mps1 were in the kinase domain (Fig 2A). Mps1 has functions in spindle assembly checkpoint signaling, correction of misattached chromosomes, and spindle pole body duplication (reviewed in Liu & Winey, 2012). We were surprised to identify mutations in Mps1 as the kinase would be expected to promote rather than antagonize CPC activity, and mutations in Mps1 that suppress CPC deficiency have not previously been identified.

Intriguingly, all of the mutations in Table 1 are in essential genes, so they are most likely to be hypomorphic alleles. To determine whether the identified mutations are sufficient to rescue *bir1Δ*, we

introduced mutations from each category prior to *BIR1* deletion. In addition, we included mutations identified in the adapted strains in three other potentially interesting proteins: the inner kinetochore protein Mif2, the spindle pole body protein Spc97, and the mitochondrial signaling protein Rtg2. Rtg2 was selected because we identified three independent mutations in this protein. After selection of *bir1Δ* on 5-FOA plates, all of the tested mutations at least partially rescued growth with the exception of *mif2*, *rtg2*, and *ask1* (Fig 2B). We identified multiple mutations that suppress the *BIR1* deletion growth phenotype for each of the four major categories. To determine whether the mutants were able to rescue the chromosome missegregation phenotype of *BIR1* deletion, we measured the fidelity of minichromosome transmission with representative suppressor mutations from the outer kinetochore, SCF complex, and Mps1 categories. We did not perform any further experiments with the Sli15 mutations, as we previously characterized similar mutations (Campbell & Desai, 2013). For the SCF complex, we analyzed mutations that we identified in Cdc4, as mutations in the F-box subunit are less likely to have pleiotropic effects. Minichromosome transmission fidelity was higher than the *bir1Δ* control for mutations in all three categories, although the degree of rescue for the Mps1 mutation was not significant ($P = 0.1$, Fig 2C). We have therefore identified four categories of mutations—in the outer kinetochore, the CPC, the SCF, and Mps1—that are frequently mutated to suppress the chromosome missegregation phenotype of yeast with impaired CPC activity.

We next wanted to test whether the suppressor mutations could affect aneuploidy tolerance in addition to CIN tolerance. Suppressor mutations in the Dam1 complex, SCF complex, and Mps1 did not suppress the growth defects caused by an extra copy of either chromosome 8 or 10 (Fig EV1B). In addition, a combination of these mutations with *ubp6(E256X)* did not show any synergistic effects (Fig EV1A). To determine whether the remaining growth impairment in the further adapted strains was primarily due to aneuploidy or CIN, we added wild-type *BIR1* to a subset of the *bir1Δ-ad* and *bir1Δ-ad2* strains and tested their growth. Even in the further adapted strains, re-addition of *BIR1* greatly improved their fitness (Fig EV1C). We conclude that even though the suppressor mutations act exclusively by suppressing the CIN phenotype, the residual CIN is still the primary contributor to the growth defects in the further adapted strains.

We next wanted to determine the degree to which the identified mutations contribute to adaptation. We compared the growth of

Figure 2. Four main categories of mutations rescue *BIR1* deletion.

- A Schematics showing the location of mutations from Table 1 (red lines). Domains of interest were identified using the Saccharomyces Genome Database.
- B Serial dilutions of strains engineered with the indicated mutations identified in *bir1Δ-ad2* strains were tested for rescue of *BIR1* deletion. Ten-fold serial dilutions on the indicated media are shown. The mutations colored in blue, green, or red were selected for additional characterization.
- C Top: schematic summarizing how loss of the *URA3*-containing plasmid is used to measure relative missegregation rates. Bottom: Proportion of colonies that grow on plates with restrictive (lacking uracil) versus permissive (YPAD) media. Many of the suppressor mutants significantly increase the segregation fidelity of the minichromosome in a *bir1Δ* background. *ctf19Δ* serves as a positive-control for decreased minichromosome transmission fidelity. Statistical significance is relative to *bir1Δ* alone for three independent experiments. Means and standard deviations are shown.
- D, E Growth comparisons of *bir1Δ-ad2* strains that contain (18 strains) or do not contain (28 strains) confirmed suppressor mutations as measured by area of colony growth after serial dilution. The mean (red line) is shown. 10-fold serial dilutions were made on YPAD plates containing either 0.1% DMSO (D) or 10 μg/ml of benomyl (E).
- F Comparison of the mean number of aneuploid chromosomes per strain for *bir1Δ-ad2* with and without identified suppressor mutations.
- Data information: (ns) not significant; (*) $P < 0.05$; (**) $P < 0.01$; (***) $P < 0.001$; (****) $P < 0.0001$; unpaired *t*-test.

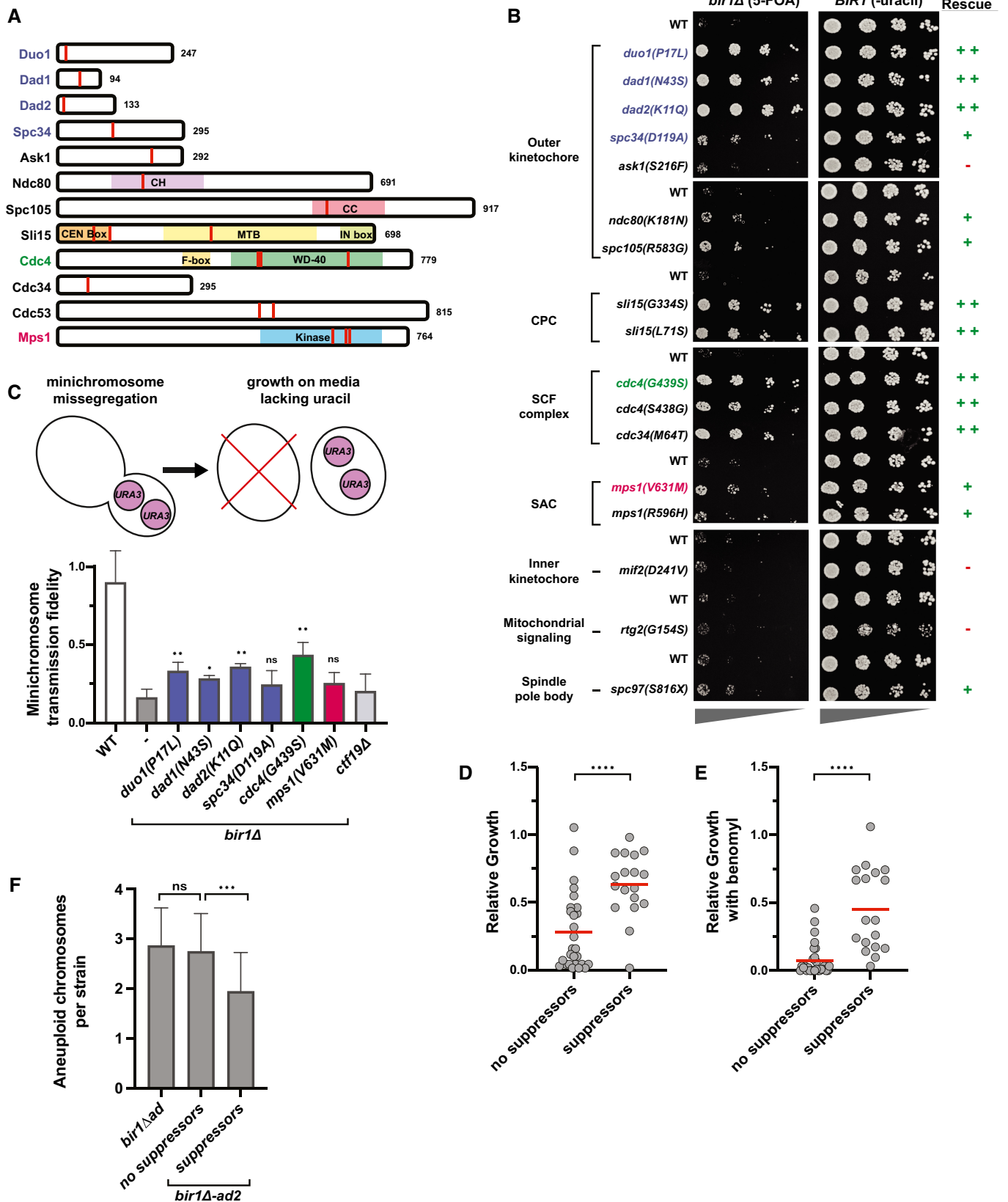


Figure 2.

bir1A-ad2 strains that either do or do not contain identified suppressor mutations. All mutations listed in Table 1 were considered suppressors for this analysis, with the exception of genes with mutations that did not rescue the *BIR1* deletion growth phenotype (*MIF2*, *RTG2*, and *ASK1*). On average, adapted strains that contain identified suppressor mutations grew substantially better than those without suppressors, suggesting that we identified most of the impactful mutations and that they contributed greatly to the adaptation (Fig 2D and E). This difference was significant either with or without the addition of benomyl. Other genetic or epigenetic changes that alter protein abundance could also contribute to adaptation under these conditions; however, the strong correlation between the identified suppressor mutations and the growth phenotype indicates that these alterations would have a relatively small contribution. Furthermore, the degree of aneuploidy is significantly reduced in the strains with suppressor mutations, indicating that these mutations decreased the need for aneuploid chromosomes to suppress the *bir1A* phenotype (Fig 2F). This decrease was seen across all of the observed aneuploid chromosomes (Fig EV1D). The aneuploidy burden in the further adapted strains was therefore reduced by decreasing the requirement for aneuploidy rather than decreasing the impact of aneuploidy on cellular fitness. These results provide a time line of events for adaptation to high rates of CIN. First, the cells acquire specific aneuploidies that suppress the CIN phenotype. The cells then acquire optimal combinations of aneuploidies (Ravichandran *et al*, 2018). Next, point mutations arise that more specifically target the source of the CIN leading to a reduction in CIN. Finally, the level of aneuploidy decreases to relieve the fitness burden placed on the cell.

Suppressor mutations in the Dam1 complex create unattached kinetochores

We next sought to determine where in the chromosome biorientation pathway each of these categories of mutations falls. Defects in CPC activity lead to the overstabilization of kinetochore–microtubule attachments and the failure to correct attachments where both sister chromatids attach to microtubules emanating from the same pole (syntelic attachments; Biggins *et al*, 2001; Pinsky *et al*, 2006). Mutations that rescue CPC defects are therefore likely to restore the higher turnover of kinetochore–microtubule attachments. This could occur either by increasing the activity of the CPC or by decreasing the microtubule binding activity of kinetochores. To determine whether the mutations act downstream of the CPC, we tested whether they could rescue a temperature-sensitive mutation in the CPC kinase Ipl1/Aurora B. Of the mutations tested, only the Dam1c mutants significantly rescued *ipl1-321* at the restrictive temperature (Fig 3A). Although the Dam1c suppressor mutations rescue the temperature-sensitive *IPL1* mutation, they could not rescue a full deletion of *SLI15*, suggesting that they do not completely bypass the need for CPC activity (Fig EV2A). These results indicate that the Dam1c mutations affect the pathway downstream of the CPC, whereas the SCF complex and Mps1 potentially affect the CPC itself.

If the mutations rescue by globally destabilizing kinetochore–microtubule attachments, then the number of unattached kinetochores should increase even in the presence of Bir1. Since unattached kinetochores trigger the spindle assembly checkpoint, we first determined whether the mutations induce a delay in mitosis.

None of the identified mutations showed substantial changes in cell cycle duration, as measured by the sustained accumulation of large budded cells over time after release from synchronization in G1 (Fig EV2B). These mutations therefore do not maintain sustained checkpoint activity. As a more sensitive assay, we monitored the presence of unattached kinetochores by measuring the frequency of cells with foci of the checkpoint protein Bub3 that colocalize with kinetochore clusters. For this assay, we only counted cells that have two kinetochore clusters that are separated yet still in close proximity, indicative of a stage around the prometaphase to metaphase transition. At this stage, three of the four Dam1c mutations resulted in significantly more cells with Bub3-mNeonGreen foci than the wild-type control (Fig 3B). By contrast, suppressor mutations in *Cdc4* and *Mps1* did not increase the frequency of Bub3 foci. We conclude that suppressor mutations in the Dam1 complex transiently increase the number of unattached kinetochores, likely through increased kinetochore–microtubule attachment turnover.

The suppression of the *bir1A* chromosome missegregation phenotype through an increase in unattached kinetochores in Dam1 complex mutants suggests that there is a restoration of the balance between microtubule attachment and detachment when both mutations are combined. If this were the mechanism of rescue, then we would expect that in the absence of *BIR1* deletion, the increase in kinetochore–microtubule attachment turnover in the Dam1 mutants would overly destabilize attachments and increase the chromosome missegregation rate. To test this, we measured the rate of minichromosome transmission in strains that have suppressor mutations and wild-type *BIR1*. Similar to the results of the Bub3 foci counts, three of the four Dam1c mutants showed a significant decrease in minichromosome transmission fidelity (Fig 3C). The *Cdc4* and *Mps1* mutations had no measurable effect. The Dam1c mutation that did not show a significant result in either the unattached kinetochore or chromosome segregation assays, *spc34(G439S)*, also had the weakest rescue of growth following *BIR1* deletion (Fig 2B). Overall, these results demonstrate that mutations in outer kinetochore proteins rescue deficient CPC activity by destabilizing kinetochore–microtubule attachments. By contrast, *Cdc4* and *Mps1* suppressor mutations act through an alternative mechanism that does not directly affect the stability of kinetochore–microtubule attachments.

Dam1c suppressor mutations have similar phenotypes to a phosphomimic mutation that decreases Dam1c microtubule binding

Phosphomimics of Ipl1 phosphorylation sites on the Dam1 subunit of the Dam1 complex were previously shown to partially rescue *ipl1-ts* mutants (Cheeseman *et al*, 2002). These phosphosites include serine 20 (*dam1(S20D)*) near the N-terminus and three serines (S257, S265, S292, *dam1(3D)*) closer to the C-terminus of the protein (Fig 4A). The two phosphomimic mutants change the serines to negatively charged aspartic acid residues. The S20D mutation has been demonstrated to reduce microtubule binding *in vitro*, whereas the 3D mutant results in activation of the mitotic checkpoint (Jin & Wang, 2013; Sarangapani *et al*, 2013). To determine whether the identified suppressor mutations function similarly to the phosphomimics, we first determined whether the *dam1*

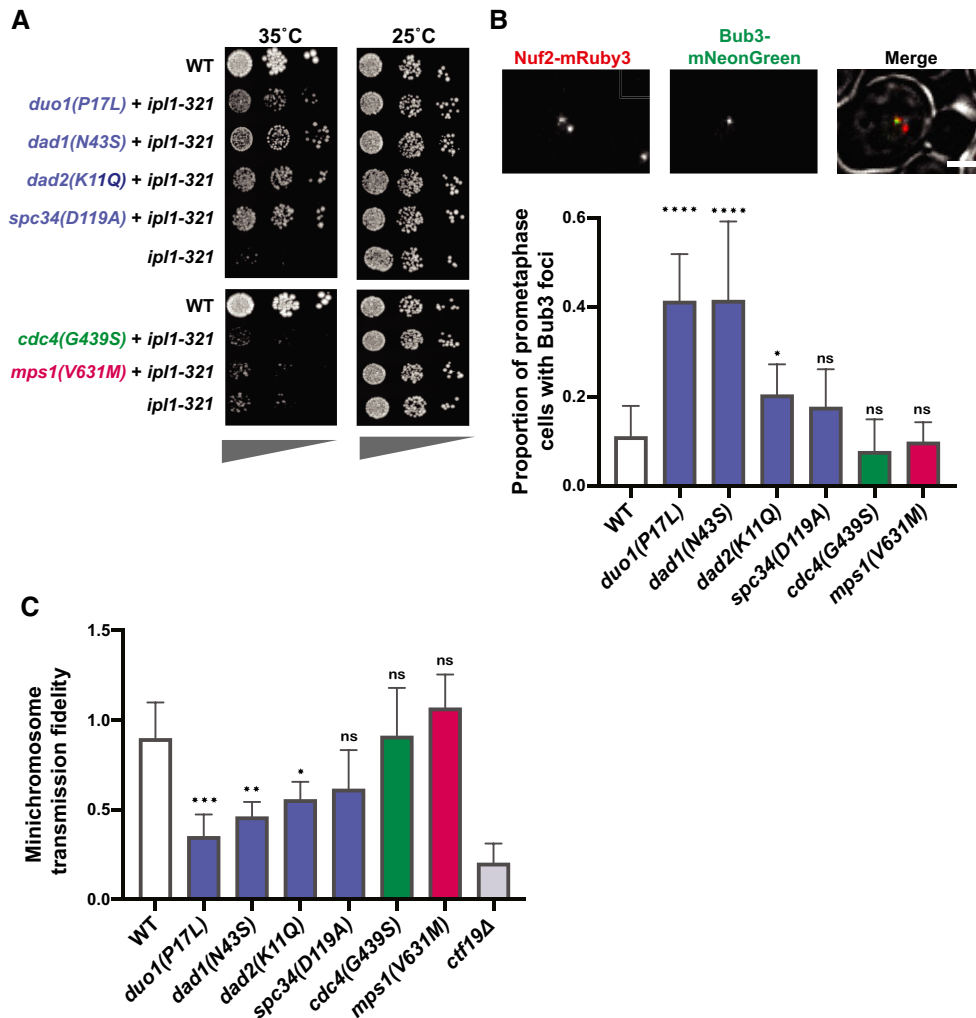


Figure 3. Suppressor mutations in the Dam1 complex result in elevated spindle assembly checkpoint activity and minichromosome missegregation.

A Serial dilutions on YPAD media at the permissive (25°C) or restrictive (35°C) temperatures for the *ipl1-321* mutation. The suppressor mutations from the Dam1c (blue) were the only mutants that rescued viability at the restrictive temperature.

B Top: representative images showing Bub3-mNeonGreen localization to kinetochores (Nuf2-mRuby3), indicating spindle assembly checkpoint activation in wild-type yeast. Scale bar is 2 μm. Bottom: quantification of the proportion of prometaphase cells with Bub3-mNeonGreen foci. Only the mutations in Dam1 complex (blue) show a significant increase in SAC activity. Data are from at least five independent experiments. Means and standard deviations are shown.

C Proportion of colonies that grow on plates with restrictive (lacking uracil) versus permissive (YPAD) media after 24 h growth under permissive conditions with a *URA3*-containing plasmid. The suppressor mutations in the Dam1c (blue) show a significant reduction of minichromosome segregation fidelity. Data are from three independent experiments. Means and standard deviations are shown.

Data information: (ns) nonsignificant; (*) $P < 0.05$; (**) $P < 0.01$; (***) $P < 0.001$; (****) $P < 0.0001$; unpaired t-test.

(*S20D*) or *dam1(3D)* mutations rescue *BIR1* deletion. Intriguingly, *dam1(S20D)* rescues *BIR1* deletion but *dam1(3D)* does not, indicating that these mutants are mechanistically distinct (Fig 4B). Both mutations increase the frequency of Bub3 foci in prometaphase cells, similarly to the Dam1c suppressor mutations that we identified (Fig 4C). However, the *3D* mutant shows a strong cell cycle delay, further indicating that it differs from the other Dam1c mutants in either mechanism or severity (Fig 4D). Despite the delay, the *3D* mutant does not affect minichromosome transmission fidelity (Fig 4E). This mitotic delay without any decrease in chromosome segregation fidelity has been previously reported for the *dam1(3D)* mutation and may indicate a defect in SAC silencing

after chromosome biorientation (Jin & Wang, 2013). The *dam1(S20D)* mutation, however, does show a decrease in minichromosome transmission in line with the suppressor mutations (Fig 4E). We conclude that the mutations in the Dam1 complex that adapt to suppress *BIR1* deletion have a similar phenotype to the *dam1(S20D)* mutation. Intriguingly, the *S20D* phosphomimic mutation was shown to disrupt microtubule binding of kinetochores *in vitro*, whereas the triple serine phosphomimic (*3D*) mutant maintained wild-type microtubule binding activity (Sarangapani et al, 2013). The similarity in phenotype between the suppressor mutations and *dam1(S20D)* suggests that the suppressor mutations may also directly decrease kinetochore–microtubule affinity.

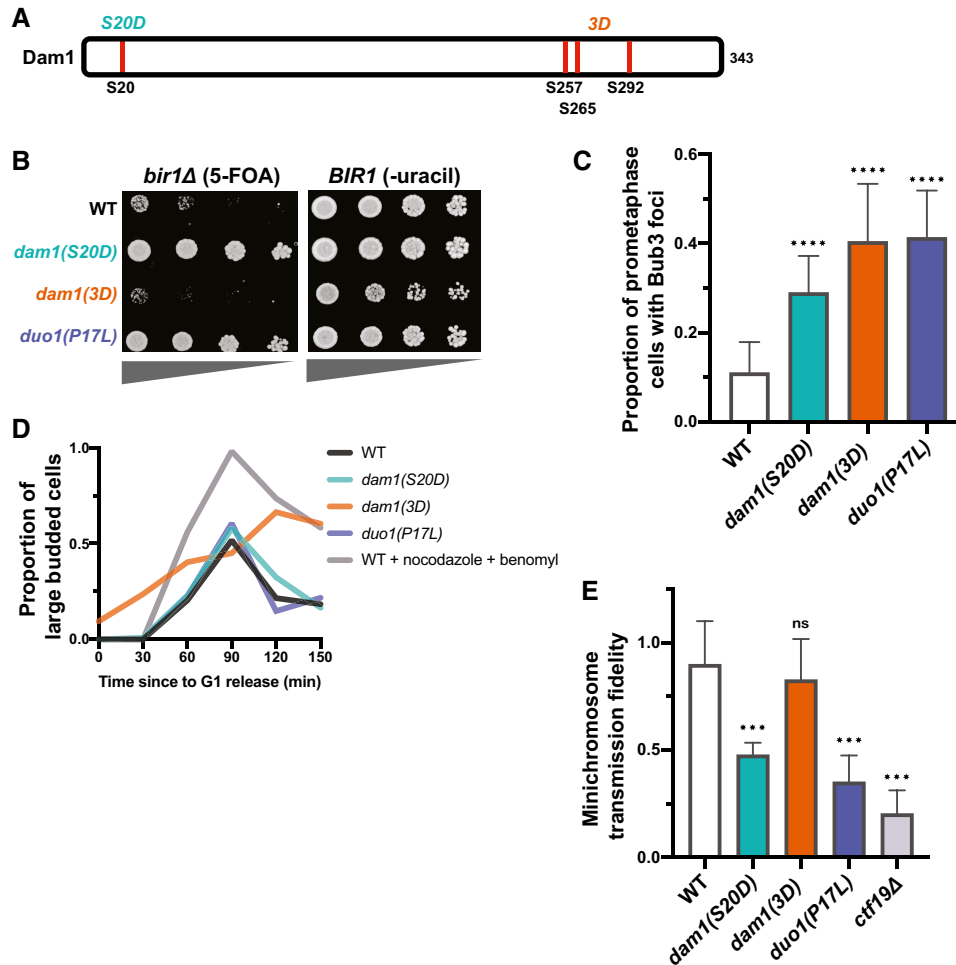


Figure 4. Suppressor mutations in the Dam1 complex have phenotypes similar to the *dam1(S20D)* phosphomimic mutation.

- A** A schematic showing the relative locations of the Ipl1 phosphosites in Dam1 that are mutated to aspartic acid in the phosphomimics.
- B** Serial dilutions of strains engineered with the indicated mutations were tested for rescue of *BIR1* deletion. Ten-fold serial dilutions on the indicated media are shown. *dam1(S20D)* rescues loss of CPC activity to a similar extent as a suppressor mutant in Duo1.
- C** Quantification of the proportion of prometaphase cells with Bub3-mNeonGreen foci localized to kinetochores (Nuf2-mRuby3), indicating SAC activation in all three mutant strains. Data are from at least five independent experiments. Means and standard deviations are shown.
- D** Degree of cell cycle delay as measured by percentage of large budded cells over time after release from G1 arrest. Wild-type (WT) cells treated with nocodazole and benomyl were used as a positive control for mitotic arrest.
- E** Proportion of colonies that grow on plates with restrictive (lacking uracil) versus permissive (YPAD) media after 24 h growth under permissive conditions with a *URA3*-containing plasmid. Minichromosome segregation fidelity is reduced in the *dam1(S20D)* strain, similar to the *duo1(P17L)* strain. Data are from three independent experiments. Means and standard deviations are shown.

Data information: (ns) nonsignificant; (***) $P < 0.001$; (****) $P < 0.0001$; unpaired *t*-test.

If both the Dam1c suppressor mutations and *dam1(S20D)* act through destabilizing kinetochore–microtubule attachments, we hypothesized that combining the two mutants might destabilize the connections to a greater extent. Indeed, combination of either *duo1(P17L)* or *dad2(K11Q)* with *dam1(S20D)* resulted in zero viable spores after 3 days of growth (Fig EV2C). For the *duo1(P17L)*, *dam1(S20D)* double mutant, rare colonies grew up after 5 days. These double-mutant cells displayed severe minichromosome loss and a strong metaphase delay, as expected for high rates of unattached kinetochores (Fig EV2D and E). Intriguingly, the double mutant was able to rescue loss of *IPL1* activity to an extent even greater than the single mutants (Fig EV2F). However,

the reverse interaction was not observed, as the *ipl1-321* mutation did not improve the growth of the *duo1(P17L)*, *dam1(S20D)* double mutant at the restrictive or permissive temperature. This could potentially be due to Ipl1 mutations preferentially stabilizing specific kinetochore–microtubule attachment states, whereas mutations in the kinetochore would destabilize all attachments indiscriminately. We conclude that the suppressor mutations in the Dam1 complex and the *dam1(S20D)* mutant both act by destabilizing kinetochore–microtubule attachments. The combination of the mutants increases the severity of the phenotype to create an extended spindle assembly checkpoint arrest and cell death.

Dam1c suppressor mutations lie proximal to multimerization interfaces and decrease spindle localization *in vivo*

To determine a potential mechanism of action for the Dam1c suppressor mutations, we mapped them onto the existing crystal structure of the *Chaetomium thermophilum* version of the complex (Jenni & Harrison, 2018). Three of the mutations are in helices that lie near interfaces of oligomerization between Dam1c decamers. *spc34(D119A)* is found in a region that corresponds to a short helix that forms part of interface 1. The *dad1(N43S)* mutation affects a highly conserved residue that lies on the surface of interface 2 (Fig 5A). The *dad2(K11Q)* mutation affects a highly conserved lysine that is also proximal to interface 2 but is not directly on the surface. The *duo1(P17L)* mutation lies in a region outside of the crystal structure. However, the affected residue would likely be near the N-terminal part of Duo1, which resides in interface 1. These interfaces are proposed to be important for the ring formation that allows the complex to encircle microtubules. It has been noted that serine 20 of the Dam1 protein is potentially also located in the vicinity of interface 1 (Jenni & Harrison, 2018). These results suggest that the suppressor mutants could act by limiting higher order oligomerization of the Dam1 complex.

The oligomerization of the Dam1 complex into rings is primarily associated with microtubule binding (Miranda *et al*, 2005; Westermann *et al*, 2005). We therefore determined whether the Dam1c mutants affect the localization of the complex to microtubules and kinetochores. We measured the amount of the Dam1 complex member Dad3 labeled with the fluorophore mNeonGreen at prometaphase and anaphase spindles in the presence of the suppressor mutants. The intensity of Dad3-mNeonGreen was significantly reduced at both prometaphase kinetochores/spindles and anaphase spindles for the three Dam1c suppressor mutations with the strongest rescue phenotypes (Fig 5B and C). The *dam1(S20D)* mutation also has a significant decrease in Dad3 localization in prometaphase. No significant decreases in Dad3 spindle localization were observed for *cdc4(G439S)* or *mps1(V631M)*. Interestingly, the decrease in localization for the Dam1c mutants was much more pronounced along the anaphase spindle than at anaphase kinetochores (Fig 5D). The maintenance of strong localization at kinetochores

suggests that the localization phenotypes could result from defects in microtubule binding rather than kinetochore association. We conclude that the Dam1c suppressor mutations decrease the amount of Dam1 complex at microtubules and this potentially occurs by decreasing the ability of the complex to oligomerize.

Mps1 suppressor mutations do not act through previously established pathways

We next wanted to determine how the Mps1 mutations rescue *BIR1* deletion. Mps1 kinase functions in activating the spindle assembly checkpoint at unattached kinetochores and recruiting the CPC to the inner centromere for chromosome biorientation (Weiss & Winey, 1996; van der Waal *et al*, 2012). In yeast, it also has an essential function in spindle pole body duplication (Winey *et al*, 1991). Disruption of any of these functions would be expected to decrease, rather than increase, the ability of cells to function with reduced CPC activity. One possible explanation for this would be if the Mps1 suppressor mutations have a gain-of-function phenotype that increases the kinase's activity. We therefore tested whether the Mps1, Cdc4, and Dam1c suppressors have gain-of-function activity by determining whether they have a dominant phenotype in the heterozygous state. Only the Dam1c mutation *duo1(P17L)* had any improved growth when heterozygous, indicating that neither the Cdc4 nor the Mps1 mutations are gain of function (Fig EV3A). To determine whether the suppressor mutations affect the ability of Mps1 to activate the spindle assembly checkpoint, we measured the percentage of cells with Bub3-mNeonGreen foci either with or without the addition of nocodazole to depolymerize microtubules and create unattached kinetochores. The levels of Bub3 foci were unaffected by the *mps1(V631M)* mutation in either the presence or the absence of nocodazole, demonstrating that the mutant cells are capable of activating the spindle assembly checkpoint (Fig EV3B).

Since the Mps1 suppressor alleles have a recessive, partial loss-of-function phenotype and the mutations are located in the kinase domain, we next tested whether a partial loss of Mps1 kinase activity can rescue *BIR1* deletion. We used a mutation in the kinase domain that renders it sensitive to ATP analogs (Jones *et al*, 2005). This mutation, *mps1-as1*, decreased the doubling time of *bir1Δ* cells

Figure 5. Suppressor mutations in the Dam1 complex reduce spindle localization.

- A View of the *Chaetomium thermophilum* Dam1c-ring, with focus on two adjacent protomers (labeled decamers 1 and 2). Interfaces 1 and 2 between adjacent decamers are shown with the blue dashed boxes as previously identified by Jenni & Harrison (2018). Mutations in the *Saccharomyces cerevisiae* proteins have been labeled based on sequence homology with *C. thermophilum*. Mutations within the structure are depicted as solid circles. Those that are located outside of the structured domains are shown as open-circles. Suppressor mutations identified in this study are colored magenta, and the residues mutated in the Dam1 phosphomimics are colored green. The marked residues are the closest approximations of the residues mutated in *S. cerevisiae*. N43 of Dad1 is conserved in *C. thermophilum*. The Dad2 residue K11 in *S. cerevisiae* is homologous to K35 in *C. thermophilum*. D119 of Spc34 maps to a short helix that contains H117 in *C. thermophilum*. The bottom right shows the location of the Dad1 residue N43 on the surface of interface 2. Images were made using ChimeraX (Pettersen *et al*, 2021).
- B Left: representative images showing the localization of Dad3-mNeonGreen (Dam1c member) and Nuf2-mRuby3 (kinetochore marker) in prometaphase cells. Scale bar is 2 μ m. Right: quantification of the intensity of Dad3-mNeonGreen at kinetochores/spindles in prometaphase cells. Each individual point on the graph represents a single measurement of Dad3-mNeonGreen intensity; up to 10 measurements per replicate. Data are from five independent experiments.
- C Left: representative images showing the localization of Dad3-mNeonGreen (Dam1c member) and Nuf2-mRuby3 (kinetochore marker) in anaphase cells. Scale bar is 2 μ m. Right: quantification of the intensity of Dad3-mNeonGreen at the spindle in anaphase cells. The intensity was measured in the middle of the spindle using a perpendicular line-scan. Each individual point on the graph represents a single measurement of Dad3-mNeonGreen intensity; up to 10 measurements per replicate. Data are from five independent experiments.
- D Quantification of the intensity of Dad3-mNeonGreen at kinetochores in anaphase cells. Kinetochore position was based on Nuf2-mRuby3 localization. The differences in localization at the anaphase kinetochores are much weaker than those measured along the spindle (Fig 5C). Each individual point on the graph represents a single measurement of Dad3-mNeonGreen intensity; up to 10 measurements per replicate. Data are from five independent experiments. The mean (red line) is shown.

Data information: (ns) nonsignificant; (*) $P < 0.05$; (**) $P < 0.01$; (***) $P < 0.001$; (****) $P < 0.0001$; unpaired t-test.

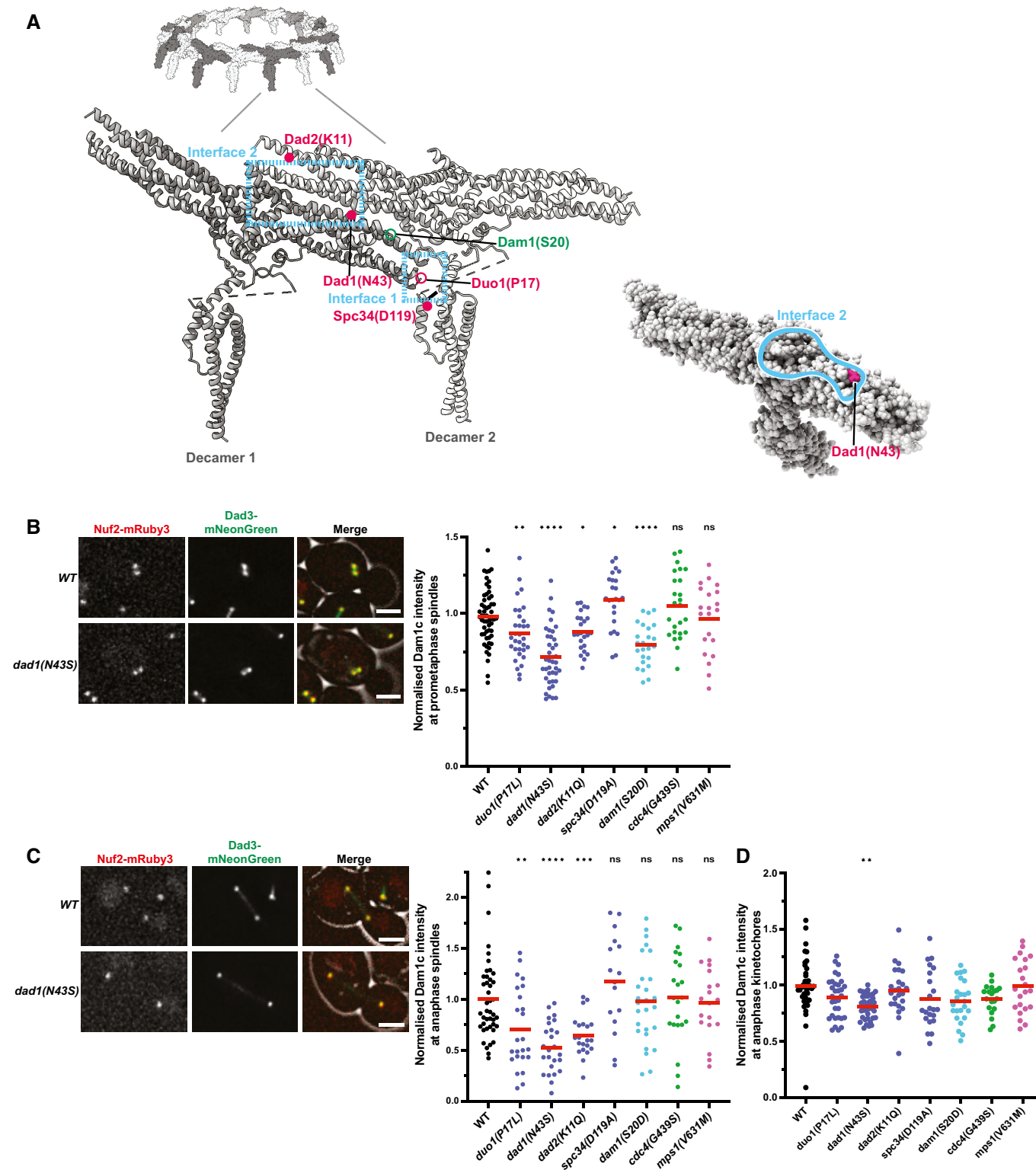


Figure 5.

to a similar extent to the suppressor mutation *mps1(V161M)* even in the absence of the small molecule inhibitor (Fig EV3C). This result suggests that the analog-sensitive mutation partially decreases kinase activity on its own, as was previously observed for similar

alleles in other kinases (Bishop *et al*, 2000; Pinsky *et al*, 2006) and, furthermore, that the *Mps1* suppressor mutations affect its kinase activity to a comparable extent. The addition of higher concentrations of the analog inhibitor decreased growth in *mps1-as1, bir1Δ*

cells, demonstrating that too little Mps1 activity is detrimental to growth even in the absence of Bir1.

We next tested whether the Mps1 mutations are suppressing CPC activity through its phosphorylation of the Dam1 complex subunit Dam1. Mutations that prevent phosphorylation of Dam1 at S218 and S221 by Mps1 kinase decrease kinetochore–microtubule stability and partially rescue temperature-sensitive Ipl1 mutations (Shimogawa *et al*, 2006, 2010). However, we did not observe any rescue of *BIR1* deletion with these mutants (Fig EV3D). This result agrees with our experiments demonstrating that the Mps1 and Dam1c suppressor mutations act through different mechanisms (Fig 3A–C). We conclude that partial disruption of Mps1 kinase activity results in rescue of *BIR1* deletion through a currently unknown mechanism.

The SCF^{Cdc4} complex affects CPC localization to the spindle/kinetochores in prometaphase in yeast and human cells

Finally, we wanted to determine how the SCF mutations rescue *BIR1* deletion. We first tested whether a previously identified temperature-sensitive mutation in *CDC4*, *cdc4-1*, is capable of rescuing loss of Bir1. We also tested a temperature-sensitive version of another F-box protein, Met30. Both Cdc4 and Met30 affect the stability of the yeast CENP-A homolog Cse4 (Au *et al*, 2020). The *cdc4-1* mutation shows a degree of rescue nearly as strong as the suppressor mutation *cdc4* (*G439S*) (Fig 6A). By contrast, a temperature-sensitive mutation in Met30 failed to show any rescue of *BIR1* deletion, demonstrating the specificity of the suppression phenotype for SCF^{Cdc4}. We conclude that rescue of *bir1Δ* results from decreased SCF^{Cdc4} activity and is not unique to the mutations identified in our screen.

To determine how Cdc4 activity affects CPC function, we first determined whether the ubiquitin ligase directly degrades the CPC subunits Sli15 or Ipl1. We monitored Sli15 and Ipl1 protein levels in cells that were prevented from expressing new protein by the addition of cycloheximide. Sli15 and Ipl1 protein levels were unchanged by the presence of the *cdc4*(*G439S*) suppressor mutation, indicating that this mutation does not rescue *BIR1* deletion by increasing the levels of Sli15 or Ipl1 (Fig EV4A). We next tested whether the Cdc4 suppressor mutations change the localization of the CPC. The *cdc4* (*G439S*) mutation significantly increased CPC localization to prometaphase spindles/kinetochores by ~50% (Fig 6B). Sli15 expression levels were also unaffected by the mutation at this cell cycle stage, suggesting that the SCF specifically affects CPC localization (Fig EV4B). We wanted to determine whether this mutant also rescues CPC localization in *bir1Δ* cells. However, *bir1Δ* greatly reduces Sli15 expression (Campbell & Desai, 2013), so we instead determined

whether *cdc4*(*G439S*) rescues localization after depletion of Sgo1, the upstream recruiter of Bir1 to the inner centromere (Fig 1A). When compared to wild-type *CDC4*, mNeonGreen-Sli15 localization in *cdc4* (*G439S*) mutant cells was significantly increased in prometaphase after Sgo1 depletion, demonstrating that this increase in CPC localization is independent of the Sgo1 recruitment pathway that acts through Bir1 (Fig. 6B). Intriguingly, the effect of *cdc4*(*G439S*) on Sli15 localization is only observed prior to anaphase, as the localization differences are no longer observed later in mitosis (Fig EV4C). This suggests that the SCF complex specifically affects CPC localization during chromosome biorientation.

We next tested whether mutations in the human homolog of Cdc4, FBXW7, also affect the accumulation of the CPC at the inner centromere. We therefore engineered the sole copy of FBXW7 in the haploid HAP1 chronic myeloid leukemia cell line with the equivalent of the G439S point mutation in the WD-40 domain that we identified in adapted *bir1Δ* cells (Fig EV5A and B). Of note, mutations in this region of the protein are frequently observed in uterine and colon cancer (Yeh *et al*, 2018). This mutation (G437S in humans) resulted in a slight increase in colony size, consistent with the function of FBXW7 as a suppressor of cell cycle entry (Fig EV5C). Intriguingly, all three cell lines engineered with this mutation showed an increase in Aurora B staining at the inner centromere in prometaphase (Fig 6C). This ~50% increase is similar to what we observe in yeast, indicating that this function of the SCF complex in CPC localization is conserved. We conclude that SCF^{Cdc4/FBXW7} activity limits the recruitment of the CPC to the spindle and/or kinetochores and that reduction of this function partially restores CPC localization when the inner centromere recruitment pathway is disrupted.

Discussion

In cancers, cells with high levels of CIN and aneuploidy often have overstabilized kinetochore–microtubule connections (Bakhoum *et al*, 2009a). Although the mechanisms that cause this phenotype are still largely unclear, one way to decrease microtubule turnover at the kinetochore is through decreased CPC activity (Cimini *et al*, 2006). In this study, we identify multiple mechanisms that cells use to adapt to the overstabilization of microtubules resulting from the deletion of the CPC subunit Bir1/Survivin. We determined that *bir1Δ* suppressor mutations act through two distinct mechanisms. The first mechanism involves mutations in proteins that directly attach the kinetochore to microtubules; such mutations were identified in five of 10 subunits of the Dam1 complex. The second

Figure 6. Cdc4 limits CPC localization in prometaphase independently of Sgo1.

- A Serial dilutions of strains engineered with the indicated mutations were tested for rescue of *BIR1* deletion. Ten-fold serial dilutions on the indicated media are shown. The *met30-6* and *cdc4-1* alleles are temperature-sensitive. Two independent clones of each of these alleles are shown. The serial dilutions were performed at the permissive temperature (20°C).
- B The amount of mNeonGreen-Sli15 (CPC member) located at kinetochores (Nuf2-mCherry) was measured in prometaphase. Sgo1 was depleted by placing it under a galactose-inducible promoter and switching to glucose-containing media (YPAD). Representative images are on the left. Scale bar is 2 μm. Averages from three independent experiments are shown.
- C Measurements of Aurora B intensity at the inner centromere of prometaphase kinetochores. Inner centromeres were identified as the regions directly between two centromeres (ACA staining). Images from an example WT cell are shown to the right. Scale bar is 5 μm long. Each data point is an individual chromosome. More than 15 cells for each cell line were measured across two independent experiments. The mean (red line) is shown.
- D Time line of adaptation to high levels of CIN through aneuploidy and point mutations.

Data information: (ns) nonsignificant; (*) $P < 0.05$; (***) $P < 0.001$; (****) $P < 0.0001$; unpaired t-test.

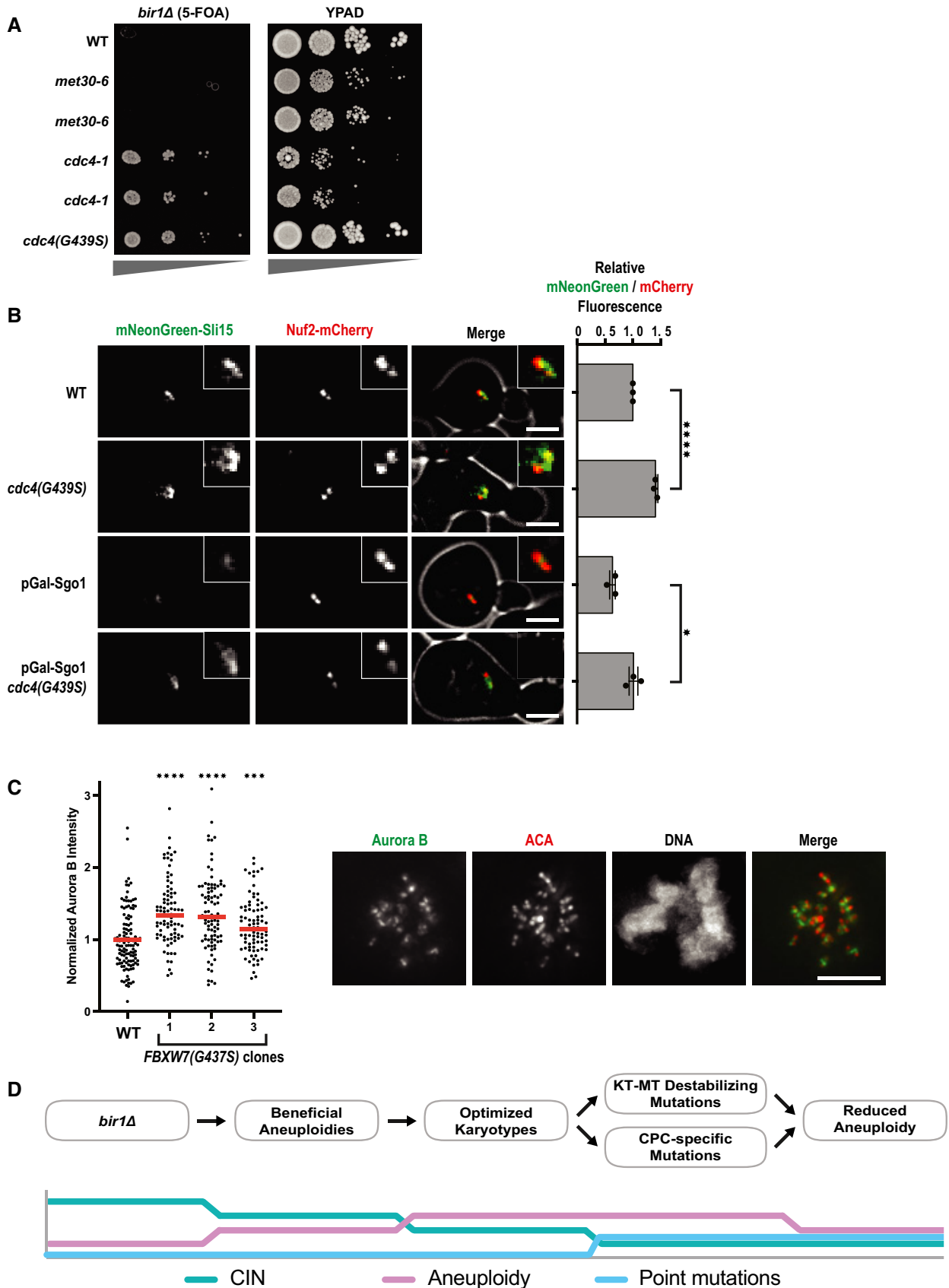


Figure 6.

mechanism results from mutations in genes that appear to affect the CPC more directly, which includes members of the SCF complex, the kinase Mps1, and the CPC member Sli15.

All of the suppressor mutations that we identified decrease the levels of CIN that result from *BIR1* deletion. Notably, we did not identify mutations whose function suggests that they allow for the greater tolerance of aneuploidy. Furthermore, a mutation in the gene *UBP6* that was previously demonstrated to reduce the negative effects of aneuploidy did not rescue *BIR1* deletion (Torres *et al*, 2010). However, mutation of *UBP6* was previously shown to improve the growth of only a subset of aneuploid chromosomes (5, 8, 9, and 11). Of these chromosomes, only aneuploidy of chromosome 8 is frequently observed in strains adapted to *bir1Δ*. Therefore, aneuploidy-tolerating mutations could potentially improve the growth of cells with other sources of CIN that adapt through different aneuploid chromosomes. In addition, the dynamics of CIN adaptation and the subsequent underlying mechanisms behind coping with CIN could vary in other strain backgrounds that may be more inherently tolerant of CIN.

In our adaptation experiments, we identified mutations in three different kinetochore complexes that directly bind to microtubules. The majority of these mutations were in the Dam1 complex. These mutations decrease the localization of the complex to microtubules and likely interfere with the complex's ability to oligomerize. The cellular phenotypes that we observe for these mutations are consistent with increased turnover of kinetochore microtubules. In vertebrates, kinetochore–microtubule turnover can be increased through the overactivation of the kinetochore-localized kinesins MCAK and Kif2b (Walczak *et al*, 1996; Kline-Smith & Walczak, 2002; Bakhomou *et al*, 2009b). Overexpression of either of these kinesins decreases the mitotic errors observed in some cancer cell lines (Bakhomou *et al*, 2009b). Furthermore, adaptation of human cells to a drug that activates MCAK resulted in cells with decreased Aurora B activity (Orr *et al*, 2016). Together, these results all point to the importance of a balance between Aurora B activity and other factors that affect the stability of connections between kinetochores and microtubules.

Mps1 is a highly conserved kinase that functions in sensing unattached kinetochores. Mps1 phosphorylates Spc105/Knl1 on MELT repeats, which recruits the spindle assembly checkpoint proteins Bub1 and Bub3/BubR1. CPC mutations have synthetic growth defects with spindle assembly checkpoint mutations, indicating that decreased SAC activity does not generally rescue CPC mutants (Ng *et al*, 2009). Bub1 binding to Spc105/Knl1 also contributes to the localization of the CPC to the inner centromere, which is one of the key locations for its function in chromosome biorientation. Bir1 is required for the CPC to bind to the inner centromere, so this targeting function of Mps1 should not affect cells with *BIR1* deletion (Makrantonis & Stark, 2009; Shimogawa *et al*, 2009). In budding yeast, Mps1 has an additional essential function in spindle pole body duplication. Interestingly, we would predict that decreased activity of any of these three functions would make the *bir1Δ* phenotype worse, not better. We conclude that the suppressor mutations partially decrease kinase activity and rescue via an unidentified mechanism. In a large-scale screen for synthetic interactions between temperature-sensitive mutations, it was found that some combinations of *MPS1* and *IPL1* alleles had positive genetic interactions, while others had negative interactions (Costanzo *et al*, 2016). These results support the idea that a balance between Mps1

activity and CPC activity is required for accurate chromosome segregation. Additional research will be required to determine which specific functions of Mps1 and which of its substrates are responsible for rescuing *BIR1* deletion.

The SCF ubiquitin ligase complex is a key regulator of many pathways related to cell cycle entry. It degrades factors that inhibit cyclins, allowing for the activation of cyclin-dependent kinases. The human homolog of the SCF F-box protein Cdc4 is FBXW7/hCDC4. FBXW7 is a tumor suppressor that is frequently mutated in many cancer types (Spruck *et al*, 2002). This function is largely attributed to the ability of FBXW7 to target important oncogenes for degradation, including MYC and Cyclin E (reviewed in Yeh *et al*, 2018). In addition to its roles in regulating cell cycle initiation, FBXW7/Cdc4 also has functions in mitosis. In yeast, certain Cdc4 mutants arrest in mitosis prior to anaphase (Goh & Surana, 1999). More recently, it was shown that Cdc4 contributes to the degradation of the inner kinetochore protein Ame1 (Böhm *et al*, 2021). In human cells, FBXW7 mutants are sensitive to inhibitors of the spindle assembly checkpoint, demonstrating a potential function in mitosis (Bailey *et al*, 2015). However, the mechanisms by which SCF^{Cdc4} regulates mitosis are still unclear. Our screen for *bir1Δ* suppressors has uncovered a connection between the SCF^{Cdc4} complex and regulation of the CPC. These suppressor mutations in the SCF complex increase the localization of the CPC to the spindle/chromosomes in the absence of inner centromere targeting, which suggests that the SCF^{Cdc4} complex may play a role in regulating alternative mechanisms of CPC localization in early mitosis. One possibility is that the SCF complex targets the degradation of a CPC recruitment factor.

Determining how cells adapt to CIN caused by the overstabilization of kinetochore-bound microtubules has important implications in cancer. Additionally, Aurora kinase inhibitors are actively being investigated in a variety of combination therapies in both preclinical and clinical trials (reviewed in Du *et al*, 2021). It is therefore important to know how cells adapt to the overstabilization of kinetochore attachments. Here, we have outlined a time line of events that cells use to adapt to decreased Aurora B activity (Fig 6D). First, cells obtain specific aneuploidies that partially decrease CIN. Next, the aneuploid karyotypes are refined to obtain an optimal complement of aneuploid chromosomes (Ravichandran *et al*, 2018). Following adaptation through aneuploidy, specific point mutations are acquired that further decrease the rate of CIN. These point mutations can affect the CPC itself or independently increase the turnover of kinetochore microtubules. Finally, point mutations that reduce CIN in a more targeted way allow for a decrease in the number of aneuploid chromosomes.

This time line of adaptation supports the theory that aneuploidy often provides a rapid but temporary form of adaptation, as has previously been observed in yeast adapted to heat stress or a tubulin mutation (Yona *et al*, 2012; Pavani *et al*, 2021). In both of those studies, a single chromosome was gained early in the adaptation process and sometimes lost again at later time points. Here, we observe the reversion toward the euploid state for many different chromosomes resulting from a wide variety of mutations. This return to the original copy number could help explain the high prevalence of whole chromosome loss of heterozygosity (LOH) in cancers. In colorectal cancers, for example, whole chromosome LOH is extremely common, even though the chromosomes are often present in multiple copies (Thiagalingam *et al*, 2001). This theory

could help explain why the bulk of LOH events do not contain known tumor suppressor genes, as the LOH itself was not the driver event, but simply a byproduct of temporary adaptation through aneuploidy (Ryland *et al.*, 2015).

Materials and Methods

Yeast strains and media

All yeast strains and plasmids that were used in this study are listed in Table EV1. Strains were grown in yeast extract and peptone supplemented with 40 µg/ml adenine-HCl (YPA) and sugars (2% glucose: YPAD, 1% galactose and 1% raffinose: YPAGR). All strains used were made in the W303 background. Benomyl (Sigma-Aldrich, 381586), nocodazole (VWR, 487928), and 5-FOA (Chempur, 220141-70-8) were used at concentrations of 10 µg/ml, 15 µg/ml, and 1 mg/ml, respectively. All cultures were incubated at 30°C unless otherwise stated. Gene deletions were carried out as previously described (Longtine *et al.*, 1998). The engineering of specific mutations at endogenous loci was achieved using the method established by the Boone laboratory (Li *et al.*, 2011).

Tissue culture

All cell lines used in this study are listed in Table EV1. All cell lines tested negatively for mycoplasma contamination. HAP1 cell lines were cultured in a humidified growth chamber at 37°C and 5% CO₂ in Iscove's Modified Dulbecco's Medium (IMDM; Sigma-Aldrich) supplemented with 10% Fetal Bovine Serum (Thermo Fisher Scientific) and 1% (v/v) Penicillin–Streptomycin (Sigma-Aldrich).

For mutation of the endogenous FBXW7 locus in HAP1 p53⁻ cells, a CRISPR/Cas9 strategy was applied. SgRNAs were cloned into pSpCas9(BB)-2A-GFP (PX458, Addgene plasmid #48138). For homologous recombination, a repair template carrying the respective mutation and 1,000 base pair (bp) homology flanks was synthesized as gBlock gene fragment (Integrated DNA Technologies IDT) and inserted into the plasmid pmScarlet_C1 (Addgene plasmid #85042). The plasmid mix of guide RNA plasmid and the repair template was transfected into HAP1 cells using FuGENE HD (Promega). Two days after transfection, cells were sorted for the presence of Cas9 (GFP positive) and repair template (mScarlet positive). Three days later, single cells were sorted into 96-well plates. Clonal populations were expanded gradually over the course of 3 weeks. The FBXW7 mutations were identified by Sanger Sequencing, and karyotypes of the cell lines were validated by flow cytometry and whole-genome sequencing.

Flow cytometry

HAP1 cells were trypsinized and stained with 10 µg/ml Hoechst 33342 (Thermo Fisher Scientific) for 30 min at 37°C. Cells were then analyzed for their ploidy state (based on G1 haploid peaks) in PBS supplemented with 5% FBS in a FACSAria III (BD) flow cytometer.

Next-generation sequencing and data analysis

Overnight cultures of each strain were made for DNA isolation. DNA was purified with the Wizard genomic DNA purification kit

(Promega). The DNA was fragmented to ~500 bp using the Bioruptor Pico sonicator for three cycles (30 s on/off). AMPure XP beads were used for size selection, and DNA libraries were prepared using the NEBNext Ultra II DNA library preparation kit for Illumina (New England Biosciences). Approximately 14 strains per run were multiplexed with NEBNext Multiplex oligos (96 index primers) and mixed at equimolar ratios. The multiplexed samples were sequenced using the 50-bp paired-end setting on an Illumina HiSeq 2500 system at the Vienna BioCenter Next-Generation Sequencing Facility (VBCF). All the raw bam files are accessible in the Sequence Read Archive (SRA—Bioproject accession number: PRJNA870080, Table EV3). The demultiplexed datasets were then aligned to the yeast genome using Bowtie2 (version 2.2.9; <http://bowtie-bio.sourceforge.net/bowtie2>) and converted to bed files using SAMtools (version 1.3.1; <http://samtools.sourceforge.net>) and Bedtools (version 2.14, <http://bedtools.readthedocs.io>). The subsequent bed files were used to calculate chromosome copy numbers using custom-made Python scripts. To normalize for differences in chromosome sizes, only the 15 kb closest to the telomeres was used. The value for the second-lowest quartile chromosomes was used for normalization. After normalization, if the chromosome copy number of a certain chromosome was greater than 1.5, it was counted as disomic (aneuploid in a haploid cell). Larger segmental copy number changes were identified visually by binning the data into 4 kb regions. Mutations in the *bir1Δ-ad* and *bir1Δ-ad2* strains were identified by running the mpileup function with SAMtools using the output from Bowtie2 alignment. These data were filtered by quality score and read depth; the quality needed to be greater than 95 and the read depth cutoff was 300. In the next step, BCFtools (version 1.3.1) was implemented to convert the bcf files generated by mpileup (SAMtools) to variant call format (.vcf) files. Subsequently, VCFtools (version 0.1.13) was used to compare all mutations found in our test strains with mutations already identified in the parent strain. Last, a custom-made Python script generated lists containing the strain identity, the coordinates of the mutation (in base pairs), and the type of mutation (coding/noncoding, silent/missense/nonsense etc.; Ravichandran *et al.*, 2018). GOrilla gene ontology tool (<http://cbl-gorilla.cs.technion.ac.il>) was used for GO enrichment tests. The target gene list was composed of all genes with nonsynonymous mutations in the adapted strains (gene repeats included), and the background list was all 6,002 genes annotated in the *S. cerevisiae* genome. The list of CIN-related genes in the yeast genome was assembled from the Saccharomyces Genome Database by searching for six specific GO terms: colony sectoring: increased; chromosome segregation: abnormal; chromosome/plasmid maintenance: decreased rate; chromosome/plasmid maintenance: abnormal; chromosome segregation: premature; and chromosome segregation: decreased. Eight hundred and seventy-four different genes satisfied these criteria.

Growth measurements

To measure growth from serial dilutions of yeast on agar plates, the images were first binarized using a threshold that distinguished the yeast colonies from the background using ImageJ. Next, a circle was placed around the first spot in the dilution series that was not saturated in the wild-type strain, and the percentage of the area above the threshold was calculated. The same dilution and circle size were used for the measurements of each other strain on the same plate.

Microscopy

Strains were grown overnight in YPAD or YPAGR, subsequently diluted 1,000-fold in the morning into fresh media, and grown for 4–6 h to midlog phase. Cells were pelleted by brief centrifugation, washed twice with 1 ml water, and resuspended in 200 μ l water. Two microliters of cell suspension was spotted onto 1% agarose pads supplemented with complete synthetic media (SC) and 2% glucose. A coverslip was placed on top and sealed with 1:1:1 mixture by weight of paraffin (Merck), lanolin (Alfa Aesar), and Vaseline (Ferd. Eimermacher). Images were collected on a DeltaVision Ultra Epifluorescence Microscope system (Cytiva) at 30°C and a PlanApo N 60/1.42 Oil objective and a sCMOS sensor, 1,020 \times 1,020 pixels, 6.5 μ m pixel size camera. For live yeast imaging, 12 z-sections with step size of 0.5 μ m were taken. Images were deconvolved using the softWoRx software (Life Sciences Software). Counting of Bub3 foci was carried out using deconvolved images. Quantification of Dad3 and Sli15 fluorescence intensity in anaphase was performed on non-deconvolved images using ImageJ and a custom-made Python script (Fink et al, 2017). Line scans perpendicular to the spindle were used for the entire spindle in prometaphase and either at the kinetochore or in between the kinetochores in anaphase. Spindle and kinetochore position were determined using the Nuf2 localization. A Gaussian curve was then fit to the intensity measurements and the area under the curve was calculated. Sli15 localization in preanaphase was quantified by drawing a circle around the Nuf2-mCherry signal, and measuring the intensities of both mCherry and mNeonGreen signals from the same circle. Background intensities were subtracted using the measurements in a larger circle that extends outside of the spindle. All analyses (except for Fig EV4C) were obtained from images obtained from a minimum of three different days. Microscopy measurements were taken with blinded samples. Representative images are deconvolved and were contrast adjusted identically using ImageJ.

To test the localization of Sli15 to the mitotic spindle, endogenous Sli15 was put under the control of a *Gal10-1* promoter. For synchronization and depletion of endogenous Sli15, overnight cultures grown in YPAGR were diluted 1:100 into YPAGR and shaken for 2 h at 30°C. Cells were resuspended in YPAGR containing α -factor (10 μ g/ml) for 45 min at 30°C. Subsequently, the medium was exchanged with YPAD containing α -factor (10 μ g/ml) and grown for 2 h and 15 min at 30°C. Cells were then released from the G1 arrest into the cell cycle by washing twice with YPAD and resuspending in YPAD containing Pronase E (Merck). Synchronized yeast cells were released into the cell cycle and grown for 45 min at 30°C. The cells were then pelleted, washed with 1 ml sterile water, resuspended in 100 μ l sterile water, and 2 μ l cell suspension was put onto 1% agarose SC pads.

For the immunofluorescence of human cells, mitotic cells were collected by mechanical shake-off and immobilized on adhesion slides (Marienfeld) for 30 min at 37°C. Next, cells were washed once in PBS, fixed for 15 min with 4% Formaldehyde in PBS, and subsequently permeabilized using 0.5% Triton-X-100 in PBS (0.5% PBST). Cells were blocked for 1 h in 0.01% PBST + 2% Bovine Serum Albumin and co-stained overnight with rabbit monoclonal anti-Aurora B antibody (Abcam, ab45145, 1:200) and human anti-centromere antibody (Antibodies Incorporated, 15-234, 1:200). After several washes with 0.01% PBST, cells were co-stained with goat

antirabbit IgG Alexa Fluor 488 (Thermo Fisher Scientific, A32723, 1:500) and goat antihuman IgG Alexa Fluor 647 (Invitrogen, A-21445, 1:500) for 2 h. After Immunostaining, DNA was stained for 1 min with 1 μ g/ml DAPI (Thermo Fisher Scientific).

Minichromosome loss assay

Yeast strains transformed with the minichromosome pRS316 were grown to saturation overnight in SC-uracil media, diluted to a starting OD⁶⁰⁰ of 0.05, and grown for 24 h in 2 ml of YPAD media. After 24 h of growth, these strains were diluted 10⁶-fold in sterile water, and 100 μ l of each strain was plated onto an SC-uracil plate and a YPAD plate. The plates were incubated at 30°C for 48 h. Pictures taken of the subsequent colonies by a Canon EOS Digital Camera. The colony numbers were counted using the “Analyze Particles” function in ImageJ. The number of colonies on the *ura*-plates were then divided by the number that grew on the YPAD plate to obtain the measurement of transmission fidelity.

ATP-analog growth assay

Strains were grown overnight in YPAD and diluted to a starting OD⁶⁰⁰ of 0.05 in 3 ml YPAD at 25°C. The strains were given up to 4.5 h to reach exponential phase. At time point zero, the indicated amount of ATP-analog 1NM-PP1 (Merck) or DMSO was added to the strains. Immediately after drug addition, 0.5 ml of each sample was diluted 2 \times in a 1 ml cuvette to analyze the OD⁶⁰⁰ (time point 0). This was repeated every 1.5 h thereafter, for 7.5 h.

Budding index

Strains were grown overnight in YPAD media, and 100 μ l of each overnight was added to 2 ml YPAD. After allowing 1 h for recovery, 2 μ l of α -factor was added every 45 min for 2 h. Strains were then washed using fresh YPAD media mixed with Pronase E (Merck; 1:10). The number of large-budded cells was counted via light-microscopy every half an hour for 2.5 h. A total of 100 cells were counted per slide per time point.

Colony formation assay

On Day 1, 600 cells were seeded into six-well plates. The plates were incubated for 12 days. Colonies were then fixed with 4% Paraformaldehyde in PBS (Sigma-Aldrich) for 20 min, washed with water, stained for 30 min with Crystal Violet, washed with water, and dried.

Protein extraction and Western blotting

For yeast protein extraction in the cycloheximide time course, saturated overnight cultures were diluted in 30 ml YPAD in order to obtain an OD⁶⁰⁰ of 0.25. Cells were grown at 30°C while shaking until an OD⁶⁰⁰ of 0.7 was reached. At this point, cycloheximide (50 μ g/ml) was added ($t = 0$). Five milliliters aliquots was taken every 30 min for a 2 h period at 30°C. Immediately after each aliquot was taken, proteins were extracted by pelleting the cells and resuspending them in 100 μ l 5% trichloroacetic acid. Following 10-min incubation at room temperature, the cells were washed once

with 1 ml ddH₂O and resuspended in 100 µl lysis buffer (50 mM Tris, pH 7.4, 50 mM dithiothreitol, 1 mM EDTA, Complete EDTA-free protease inhibitor cocktail (Roche) and Phosstop (Roche)). Cells were vortexed for 30 min at 4°C after the addition of glass beads. Subsequently, 33 µl 4× sample buffer was added and incubated at 95°C for 5 min. For protein extractions in prometaphase cells, saturated overnight cultures were diluted in 10 ml YPAGR in order to obtain an OD⁶⁰⁰ of 0.25. Cells were then synchronized as described as for the microscopy experiments. Sixty minutes after G1 release, proteins were extracted by resuspending cells in 100 µl 0.2 M NaOH. After 5-min incubation at room temperature, cells were resuspended in 100 µl H₂O. Thirty-three microliters of 4× sample buffer was added and incubated at 95°C for 5 min. Samples were stored at −20°C. For immunoblots, the following antibodies were used: rat anti-HA-clone 3F10 (Roche), mouse anti-PGK1 monoclonal 22C5D8 (Thermo Fisher Scientific). Membranes were probed with the corresponding secondary antibodies: antirat IgG-HRP-lined (Cell Signaling Technology) or antimouse IgG-HRP-linked (Cell Signaling Technology). Immunoblots were quantified using ImageJ.

Statistics

Statistical analysis was performed using the GraphPad Prism software. Details to the statistical tests used in a particular experiment are reported in the figure legends.

Data availability

All the raw bam files are accessible in the Sequence Read Archive (SRA-BioProject accession number: PRJNA870080). Information on each sample ID can be found in Table EV3.

Expanded View for this article is available [online](#).

Acknowledgements

The authors would like to thank the Campbell and Dammermann laboratories for helpful discussions and comments. We thank the Basrai and Klein laboratories for gifts of yeast strains and plasmids. The parental HAP1 p53-null cell line was kindly provided by J.I. Loizou. We acknowledge the service of the Perutz Labs BioOptics Facility, a member of the VLSI. We would also like to acknowledge the services provided to us by the VBC sequencing facility located at the VBCF. This work was supported by Vienna Science and Technology Fund (WWTF) grant VRG14-001 and Austrian Science Fund (FWF) grants Y944-B28 and W1238-B20 to CSC.

Author contributions

Matthew N Clarke: Conceptualization; data curation; formal analysis; writing – original draft; writing – review and editing. **Theodor Marsoner:** Data curation; formal analysis; writing – original draft. **Manuel Alonso Y Adell:** Data curation; formal analysis; writing – original draft. **Madhesh C Ravichandran:** Data curation; formal analysis; writing – original draft. **Christopher S Campbell:** Conceptualization; data curation; formal analysis; supervision; funding acquisition; writing – original draft; writing – review and editing.

Disclosure and competing interests statement

The authors declare that they have no conflict of interest.

References

- Ainsztein AM, Kandels-Lewis SE, Mackay AM, Earnshaw WC (1998) INCENP centromere and spindle targeting: identification of essential conserved motifs and involvement of heterochromatin protein HP1. *J Cell Biol* 143: 1763–1774
- Au W-C, Zhang T, Mishra PK, Eisenstatt JR, Walker RL, Ocampo J, Dawson A, Warren J, Costanzo M, Baryshnikova A *et al* (2020) Skp, Cullin, F-box (SCF)-Met30 and SCF-Cdc4-mediated proteolysis of CENP-A prevents Mislocalization of CENP-A for chromosomal stability in budding yeast. *PLoS Genet* 16: e1008597
- Bailey ML, Singh T, Mero P, Moffat J, Hieter P (2015) Dependence of human colorectal cells lacking the FBW7 tumor suppressor on the spindle assembly checkpoint. *Genetics* 201: 885–895
- Bakhom SF, Genovese G, Compton DA (2009a) Deviant kinetochore microtubule dynamics underlie chromosomal instability. *Curr Biol* 19: 1937–1942
- Bakhom SF, Thompson SL, Manning AL, Compton DA (2009b) Genome stability is ensured by temporal control of kinetochore–microtubule dynamics. *Nat Cell Biol* 11: 27–35
- Bakhom SF, Silkworth WT, Nardi IK, Nicholson JM, Compton DA, Cimini D (2014) The mitotic origin of chromosomal instability. *Curr Biol* 24: R148–R149
- Ben-David U, Amon A (2020) Context is everything: aneuploidy in cancer. *Nat Rev Genet* 21: 44–62
- Biggins S, Bhalla N, Chang A, Smith DL, Murray AW (2001) Genes involved in sister chromatid separation and segregation in the budding yeast *Saccharomyces cerevisiae*. *Genetics* 159: 453–470
- Bishop JD, Schumacher JM (2002) Phosphorylation of the carboxyl terminus of inner centromere protein (INCENP) by the Aurora B kinase stimulates Aurora B kinase activity. *J Biol Chem* 277: 27577–27580
- Bishop AC, Ubersax JA, Petsch DT, Matheos DP, Gray NS, Blethrow J, Shimizu E, Tsien JZ, Schultz PG, Rose MD *et al* (2000) A chemical switch for inhibitor-sensitive alleles of any protein kinase. *Nature* 407: 395–401
- Böhm M, Killinger K, Dudziak A, Pant P, Jänen K, Hohoff S, Mechtler K, Örd M, Loog M, Sanchez-Garcia E *et al* (2021) Cdc4 phospho-degrons allow differential regulation of Ame1/CENP-U protein stability across the cell cycle. *eLife* 10: e67390
- Cahill DP, Kinzler KW, Vogelstein B, Lengauer C (1999) Genetic instability and darwinian selection in tumours. *Trends Cell Biol* 9: M57–M60
- Campbell CS, Desai A (2013) Tension sensing by Aurora B kinase is independent of survivin-based centromere localization. *Nature* 497: 118–121
- Cheeseman IM, Anderson S, Jwa M, Green EM, Kang JS, Yates JR, Chan CSM, Drubin DG, Barnes G (2002) Phospho-regulation of kinetochore–microtubule attachments by the Aurora kinase Ipl1p. *Cell* 111: 163–172
- Cheeseman IM, Chappie JS, Wilson-Kubalek EM, Desai A (2006) The conserved KMN network constitutes the core microtubule-binding site of the kinetochore. *Cell* 127: 983–997
- Ciferri C, Pasqualato S, Screpanti E, Varetto G, Santaguida S, Reis Dos G, Maiolica A, Polka J, De Luca JG, De Wulf P *et al* (2008) Implications for kinetochore–microtubule attachment from the structure of an engineered Ndc80 complex. *Cell* 133: 427–439
- Cimini D, Wan X, Hirel CB, Salmon ED (2006) Aurora kinase promotes turnover of kinetochore microtubules to reduce chromosome segregation errors. *Curr Biol* 16: 1711–1718
- Costanzo M, VanderSluis B, Koch EN, Baryshnikova A, Pons C, Tan G, Wang W, Usaj M, Hanchard J, Lee SD *et al* (2016) A global genetic interaction network maps a wiring diagram of cellular function. *Science* 353: aaf1420

- Du R, Huang C, Liu K, Li X, Dong Z (2021) Targeting AURKA in cancer: Molecular mechanisms and opportunities for cancer therapy. *Mol Cancer* 20: 15–27
- Fink S, Turnbull K, Desai A, Campbell CS (2017) An engineered minimal chromosomal passenger complex reveals a role for INCENP/Sli15 spindle association in chromosome biorientation. *J Cell Biol* 216: 911–923
- Gassmann R, Carvalho A, Henzing AJ, Ruchaud S, Hudson DF, Honda R, Nigg EA, Gerloff DL, Earnshaw WC (2004) Borealin: a novel chromosomal passenger required for stability of the bipolar mitotic spindle. *J Cell Biol* 166: 179–191
- Goh PY, Surana U (1999) Cdc4, a protein required for the onset of S phase, serves an essential function during G₂/M transition in *Saccharomyces cerevisiae*. *Mol Cell Biol* 19: 5512–5522
- Gordon DJ, Resio B, Pellman D (2012) Causes and consequences of aneuploidy in cancer. *Nat Rev Genet* 13: 189–203
- Gropp A, Winking H, Herbst EW, Claussen CP (1983) Murine trisomy: developmental profiles of the embryo, and isolation of trisomic cellular systems. *J Exp Zool* 228: 253–269
- Honda R, Körner R, Nigg EA (2003) Exploring the functional interactions between Aurora B, INCENP, and survivin in mitosis. *Mol Biol Cell* 14: 3325–3341
- Hose J, Escalante LE, Clowers KJ, Dutcher HA, Robinson D, Bouriakov V, Coon JJ, Shishkova E, Gasch AP (2020) The genetic basis of aneuploidy tolerance in wild yeast. *eLife* 9: e52063
- Jenni S, Harrison SC (2018) Structure of the DASH/Dam1 complex shows its role at the yeast kinetochore–microtubule interface. *Science* 360: 552–558
- Jeyaprakash AA, Klein UR, Lindner D, Ebert J, Nigg EA, Conti E (2007) Structure of a Survivin-Borealin-INCENP core complex reveals how chromosomal passengers travel together. *Cell* 131: 271–285
- Jin F, Wang Y (2013) The signaling network that silences the spindle assembly checkpoint upon the establishment of chromosome bipolar attachment. *Proc Natl Acad Sci USA* 110: 21036–21041
- Jones MH, Huneycutt BJ, Pearson CG, Zhang C, Morgan G, Shokat K, Bloom K, Winey M (2005) Chemical genetics reveals a role for Mps1 kinase in kinetochore attachment during mitosis. *Curr Biol* 15: 160–165
- Jonkers W, Rep M (2009) Lessons from fungal F-box proteins. *Eukaryot Cell* 8: 677–695
- Kalantzaki M, Kitamura E, Zhang T, Mino A, Novak B, Tanaka TU (2015) Kinetochore–microtubule error correction is driven by differentially regulated interaction modes. *Nat Cell Biol* 17: 421–433
- Kawashima SA, Tsukahara T, Langegger M, Hauf S, Kitajima TS, Watanabe Y (2007) Shugoshin enables tension-generating attachment of kinetochores by loading Aurora to centromeres. *Genes Dev* 21: 420–435
- Kawashima SA, Yamagishi Y, Honda T, Ishiguro K-I, Watanabe Y (2010) Phosphorylation of H2A by Bub1 prevents chromosomal instability through localizing shugoshin. *Science* 327: 172–177
- Klein UR, Nigg EA, Gruneberg U (2006) Centromere targeting of the chromosomal passenger complex requires a ternary subcomplex of Borealin, Survivin, and the N-terminal domain of INCENP. *Mol Biol Cell* 17: 2547–2558
- Kline-Smith SL, Walczak CE (2002) The microtubule-destabilizing kinesin XKCM1 regulates microtubule dynamic instability in cells. *Mol Biol Cell* 13: 2718–2731
- Kwon M, Godinho SA, Chandhok NS, Ganem NJ, Azioune A, Théry M, Pellman D (2008) Mechanisms to suppress multipolar divisions in cancer cells with extra centrosomes. *Genes Dev* 22: 2189–2203
- Li Z, Vizeacoumar FJ, Bahr S, Li J, Warringer J, Vizeacoumar FS, Min R, VanderSluis B, Bellay J, Devit M et al (2011) Systematic exploration of essential yeast gene function with temperature-sensitive mutants. *Nat Biotechnol* 29: 361–367
- Liu X, Winey M (2012) The MPS1 family of protein kinases. *Annu Rev Biochem* 81: 561–585
- Longtine MS, McKenzie A, Demarini DJ, Shah NG, Wach A, Brachat A, Philippsen P, Pringle JR (1998) Additional modules for versatile and economical PCR-based gene deletion and modification in *Saccharomyces cerevisiae*. *Yeast* 14: 953–961
- Makrantonis V, Stark MJR (2009) Efficient chromosome biorientation and the tension checkpoint in *Saccharomyces cerevisiae* both require Bir1. *Mol Cell Biol* 29: 4552–4562
- Miranda JLL, De Wulf P, Sorger PK, Harrison SC (2005) The yeast DASH complex forms closed rings on microtubules. *Nat Struct Mol Biol* 12: 138–143
- Ng TM, Waples WG, Lavoie BD, Biggins S (2009) Pericentromeric sister chromatid cohesion promotes kinetochore biorientation. *Mol Biol Cell* 20: 3818–3827
- Orr B, Talje L, Liu Z, Kwok BH, Compton DA (2016) Adaptive resistance to an inhibitor of chromosomal instability in human cancer cells. *Cell Rep* 17: 1755–1763
- Pavani M, Bonaiuti P, Chirolì E, Gross F, Natali F, Macaluso F, Póti Á, Pasqualato S, Farkas Z, Pompei S et al (2021) Epistasis, aneuploidy, and functional mutations underlie evolution of resistance to induced microtubule depolymerization. *EMBO J* 40: e108225
- Petersen EF, Goddard TD, Huang CC, Meng EC, Couch GS, Croll TI, Morris JH, Ferrin TE (2021) UCSF ChimeraX: structure visualization for researchers, educators, and developers. *Protein Sci* 30: 70–82
- Pinsky BA, Kung C, Shokat KM, Biggins S (2006) The Ipl1-Aurora protein kinase activates the spindle checkpoint by creating unattached kinetochores. *Nat Cell Biol* 8: 78–83
- Ravichandran MC, Fink S, Clarke MN, Hofer FC, Campbell CS (2018) Genetic interactions between specific chromosome copy number alterations dictate complex aneuploidy patterns. *Genes Dev* 32: 1485–1498
- Ryland GL, Doyle MA, Goode D, Boyle SE, Choong DYH, Rowley SM, Li J, Bowtell DD, Tothill RW, Campbell IG et al (2015) Loss of heterozygosity: what is it good for? *BMC Med Genomics* 8: 1–12
- Sansregret L, Patterson JO, Dewhurst S, López-García C, Koch A, McGranahan N, Chao WCH, Barry DJ, Rowan A, Instrell R et al (2017) APC/C dysfunction limits excessive cancer chromosomal instability. *Cancer Discov* 7: 218–233
- Sarangapani KK, Akiyoshi B, Duggan NM, Biggins S, Asbury CL (2013) Phosphoregulation promotes release of kinetochores from dynamic microtubules via multiple mechanisms. *Proc Natl Acad Sci USA* 110: 7282–7287
- Sessa F, Mapelli M, Ciferri C, Tarricone C, Arecas LB, Schneider TR, Stukenberg PT, Musacchio A (2005) Mechanism of Aurora B activation by INCENP and inhibition by hesperadin. *Mol Cell* 18: 379–391
- Shimogawa MM, Graczyk B, Gardner MK, Francis SE, White EA, Ess M, Molk JN, Ruse C, Niessen S, Yates JR et al (2006) Mps1 phosphorylation of Dam1 couples kinetochores to microtubule plus ends at metaphase. *Curr Biol* 16: 1489–1501
- Shimogawa MM, Widlund PO, Riffle M, Ess M, Davis TN (2009) Bir1 is required for the tension checkpoint. *Mol Biol Cell* 20: 915–923
- Shimogawa MM, Wargacki MM, Muller EG, Davis TN (2010) Laterally attached kinetochores recruit the checkpoint protein Bub1, but satisfy the spindle checkpoint. *Cell Cycle* 9: 3619–3628
- Spruck CH, Strohmaier H, Sangfelt O, Müller HM, Hubalek M, Müller-Holzner E, Marth C, Widschwendter M, Reed SI (2002) hCDC4 gene mutations in endometrial cancer. *Cancer Res* 62: 4535–4539
- Tanaka TU, Rachidi N, Janke C, Pereira G, Galova M, Schiebel E, Stark MJR, Nasmyth K (2002) Evidence that the Ipl1-Sli15 (Aurora kinase-INCENP)

- complex promotes chromosome bi-orientation by altering kinetochore-spindle pole connections. *Cell* 108: 317–329
- Thiagalingam S, Laken S, Willson JK, Markowitz SD, Kinzler KW, Vogelstein B, Lengauer C (2001) Mechanisms underlying losses of heterozygosity in human colorectal cancers. *Proc Natl Acad Sci USA* 98: 2698–2702
- Torres EM, Sokolsky T, Tucker CM, Chan LY, Boselli M, Dunham MJ, Amon A (2007) Effects of aneuploidy on cellular physiology and cell division in haploid yeast. *Science* 317: 916–924
- Torres EM, Dephoure N, Panneerselvam A, Tucker CM, Whittaker CA, Gygi SP, Dunham MJ, Amon A (2010) Identification of aneuploidy-tolerating mutations. *Cell* 143: 71–83
- van der Waal MS, Saurin AT, Vromans MJM, Vleugel M, Wurzenberger C, Gerlich DW, Medema RH, Kops GJPL, Lens SMA (2012) Mps1 promotes rapid centromere accumulation of Aurora B. *EMBO Rep* 13: 847–854
- Vanoosthuysse V, Prykhodzij S, Hardwick KG (2007) Shugoshin 2 regulates localization of the chromosomal passenger proteins in fission yeast mitosis. *Mol Biol Cell* 18: 1657–1669
- Walczak CE, Mitchison TJ, Desai A (1996) XKCM1: a xenopus kinesin-related protein that regulates microtubule dynamics during mitotic spindle assembly. *Cell* 84: 37–47
- Weiss E, Winey M (1996) The *Saccharomyces cerevisiae* spindle pole body duplication gene MPS1 is part of a mitotic checkpoint. *J Cell Biol* 132: 111–123
- Westermann S, Avila-Sakar A, Wang H-W, Niederstrasser H, Wong J, Drubin DG, Nogales E, Barnes G (2005) Formation of a dynamic kinetochore-microtubule interface through assembly of the Dam1 ring complex. *Mol Cell* 17: 277–290
- Winey M, Goetsch L, Baum P, Byers B (1991) MPS1 and MPS2: novel yeast genes defining distinct steps of spindle pole body duplication. *J Cell Biol* 114: 745–754
- Yeh C-H, Bellon M, Nicot C (2018) FBXW7: a critical tumor suppressor of human cancers. *Mol Cancer* 17: 115–119
- Yona AH, Manor YS, Herbst RH, Romano GH, Mitchell A, Kupiec M, Pilpel Y, Dahan O (2012) Chromosomal duplication is a transient evolutionary solution to stress. *Proc Natl Acad Sci USA* 109: 21010–21015



License: This is an open access article under the terms of the [Creative Commons Attribution](#) License, which permits use, distribution and reproduction in any medium, provided the original work is properly cited.

Expanded View Figures

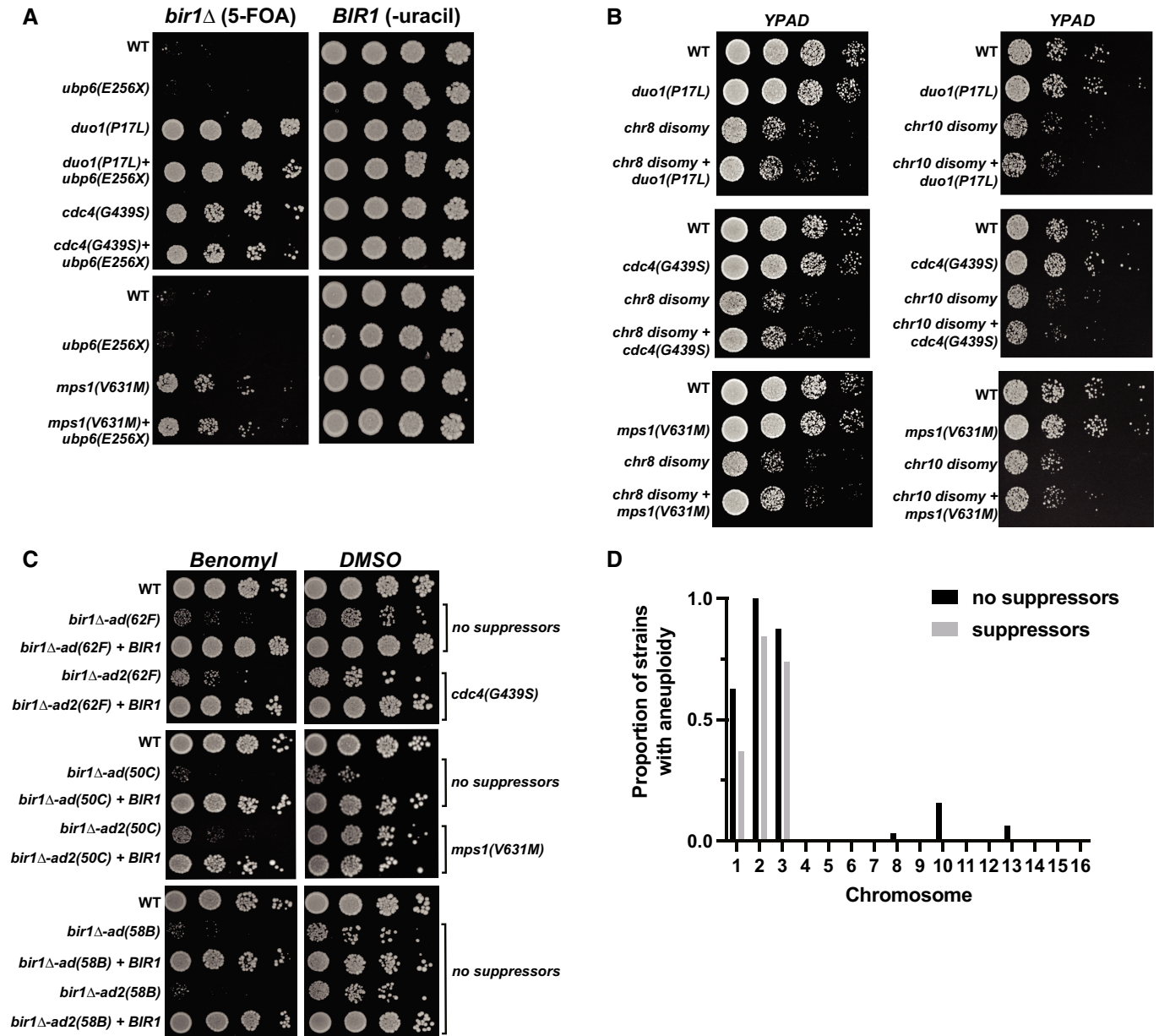


Figure EV1. CIN-related mutations in *bir1* Δ -ad2 strains are associated with decreased aneuploidy.

- A Ten-fold serial dilutions on the indicated media are shown. Strains engineered with the *ubp6(E256X)* aneuploidy tolerance mutation show no *bir1* Δ suppression. Strains with both the *ubp6(E256X)* mutation and a *bir1* Δ suppressor mutant do not additionally rescue the loss of CPC activity.
- B Ten-fold serial dilutions on the indicated media are shown. Strains have disomy of either chromosome 8 (chr8) or chromosome 10 (chr10) with or without the *bir1* Δ suppressor mutations. The combination of either type of disomy with any of the three suppressors shows no change in growth.
- C Ten-fold serial dilutions of the indicated strains were made on YPAD plates containing either 0.1% DMSO or 10 μ g/ml of benomyl. Strains were adapted to persistent loss of CPC function for different amounts of time with or without *BIR1* then restored. Those *bir1* Δ -ad strains that developed suppressor mutations after the extended growth period (*bir1* Δ -ad2(62F) and *bir1* Δ -ad2(50C)) were better able to cope with benomyl than one that did not develop suppressors (*bir1* Δ -ad2(58B)).
- D Histogram showing the proportion of strains that are aneuploid for specific chromosomes in *bir1* Δ -ad2 strains that have identified suppressor mutations, and those that do not.

Figure EV2. Double mutants of *bir1Δ* suppressors in the Dam1 complex and the *dam1(S20D)* phosphomimic have strong synthetic phenotypes.

- A Tetrad dissections performed on diploids with both *sli15Δ* and the *duo1(P17L)* did not produce any viable spores with either *sli15Δ* or a combination of *sli15Δ* and *duo1(P17L)*.
- B Cell cycle progression as measured by percentage of large budded cells over time after release from G1 arrest. None of the tested suppressor mutants cause a mitotic delay.
- C Tetrad dissections of diploids heterozygous for both a *bir1Δ* suppressor mutant and the *dam1(S20D)* phosphomimic mutant. Presence of either the suppressor mutant or *dam1(S20D)* was determined by antibiotic resistance conferred by a gene integrated downstream of the mutations (*clonNAT* and *G418* respectively). Colonies from haploid spores containing either *dad2(K11Q)*, *dam1(S20D)* or *duo1(P17L)*, *dam1(S20D)* were extremely rare. Spore viability of each genotype was counted in tetrads whose type (parental ditype, nonparental ditype, or tetratype) could be distinguished. Quantification for each mutant is from a single plate, and the WT numbers are the averages from all six plates. The representative image to the right of the graph depicts six tetrads, demonstrating examples of three tetratypes, two nonparental ditypes, and a single parental ditype. In this example, the expectant *duo1(P17L)*, *dam1(S20D)* double-mutant formed a colony from 0 out of seven spores.
- D Proportion of colonies that grow on plates with restrictive (lacking uracil) versus permissive (YPAD) media after 24 h growth under permissive conditions with a *URA3*-containing plasmid. *duo1(P17L)*, *dam1(S20D)* double mutants have a strong decrease in transmission fidelity. Data are from three independent experiments. Means and standard deviations are shown.
- E Cell cycle progression as measured by percentage of large budded cells over time after release from G1 arrest. Rare surviving *duo1(P17L)*, *dam1(S20D)* double mutants have a strong mitotic delay. Wild-type (WT) cells treated with nocodazole and benomyl were used as a positive control for mitotic arrest.
- F Serial dilution showing growth of strains containing either the double-mutant (*duo1(P17L)*, *dam1(S20D)*), the *ipl1-321* temperature-sensitive allele, or a combination of all three mutations. At the restrictive temperature (34°C), the double-mutant rescues growth of the *ipl1-321* allele. Ten-fold serial dilutions were done on YPAD plates at the indicated temperatures and were grown for 48 h.

Data information: (ns) not significant; (*) $P < 0.05$; (**) $P < 0.01$; (***) $P < 0.001$; unpaired *t*-test.

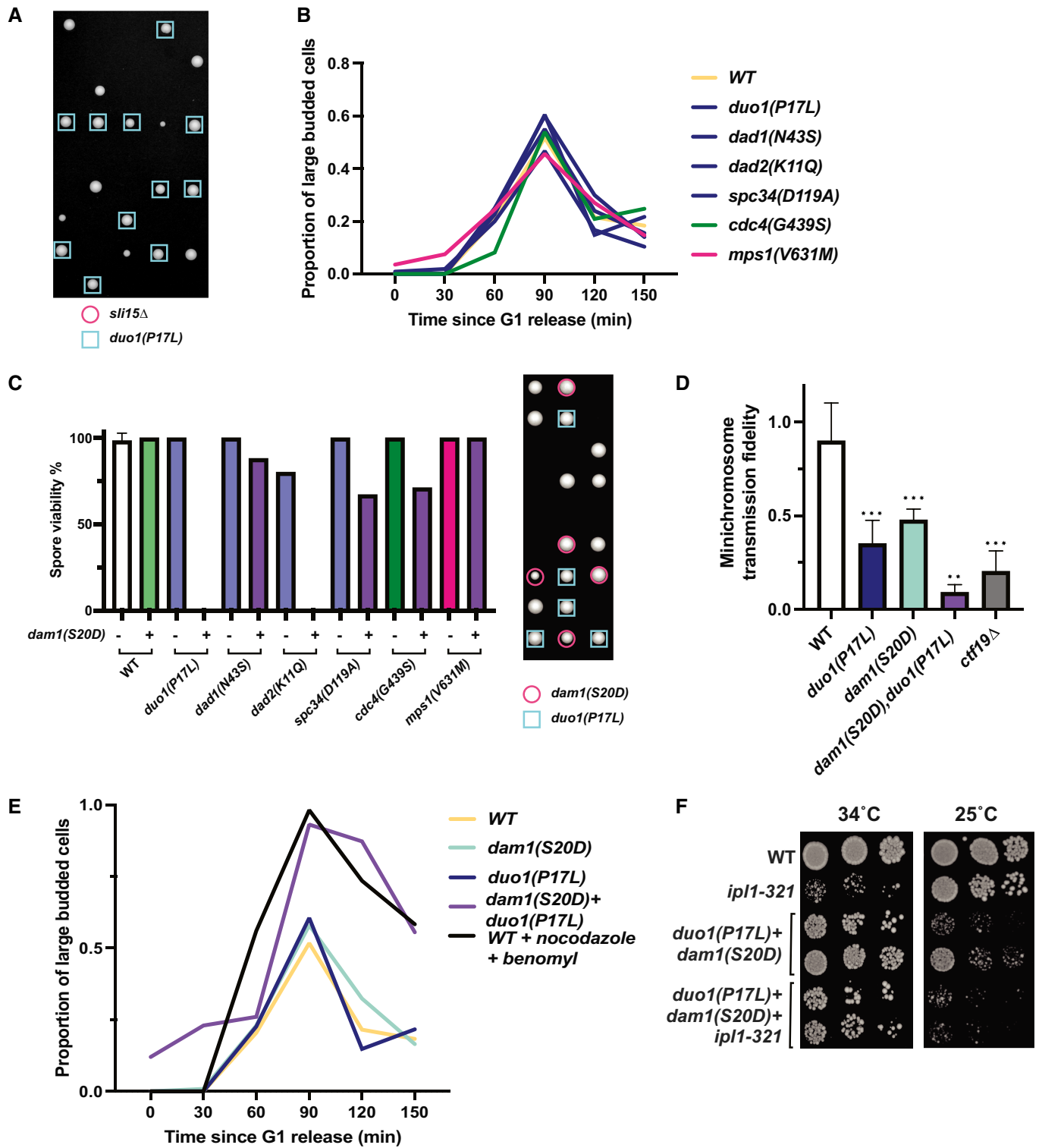


Figure EV2.

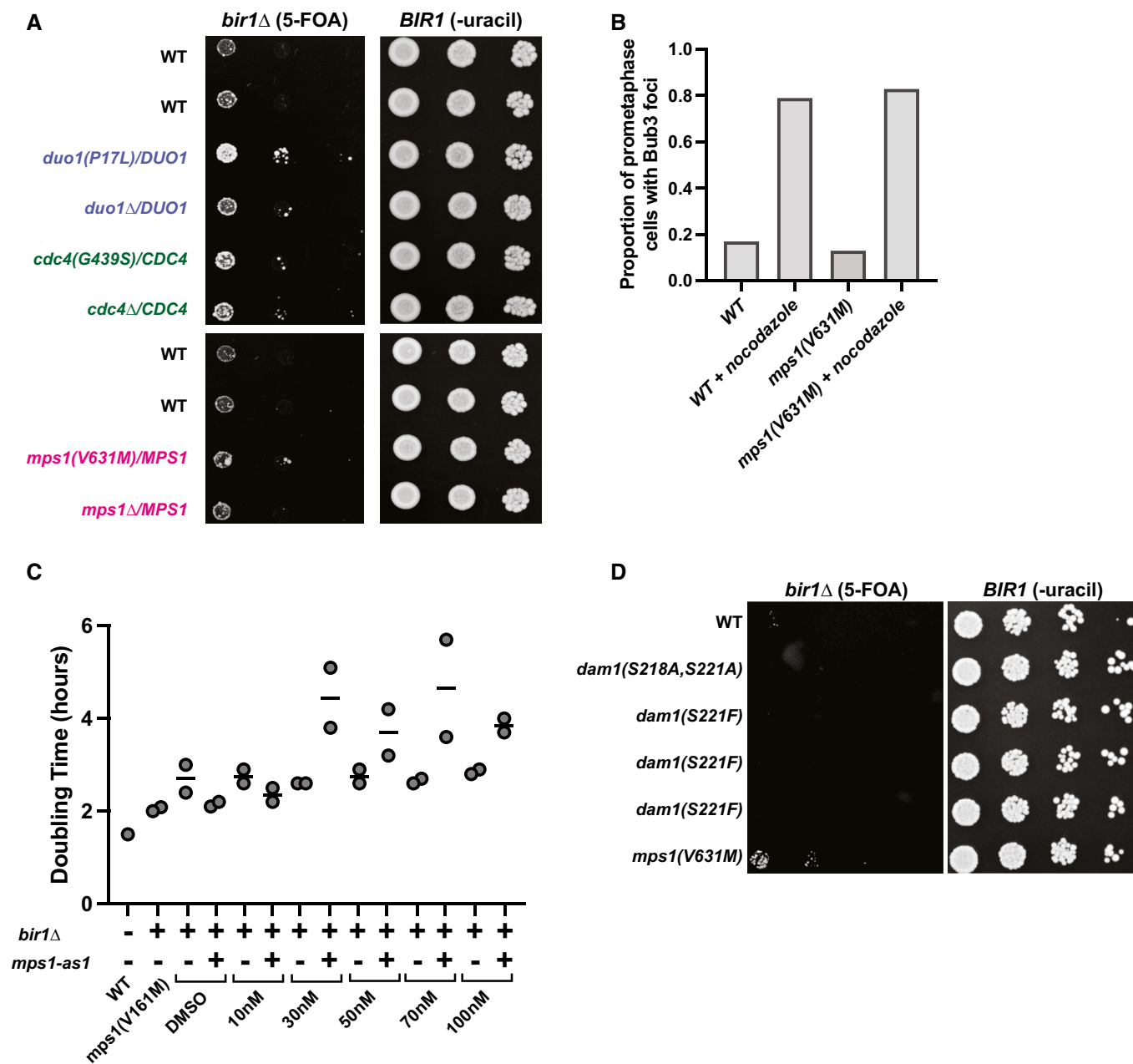


Figure EV3. Suppression of *bir1* Δ by *Mps1* mutations occurs through decreased kinase activity that does not inhibit spindle assembly checkpoint activity.

- A Ten-fold serial dilutions on the indicated media are shown. Strains engineered with the indicated mutations were tested for rescue of *BIR1* deletion. Diploid strains were heterozygous for either an identified suppressor mutation or a full deletion of the gene.
- B Quantification of the proportion of prometaphase cells with Bub3-mNeonGreen foci with or without 15 μ g/ml nocodazole. The *mps1*(V631M) mutation does not affect the percentage of cells with spindle assembly checkpoint foci. Data are from a single experiment.
- C Growth assays conducted with an ATP-analog (1NM-PP1) that specifically inhibits the *mps1-as1* allele. Strains with wild-type *Mps1* were not affected by the inhibitor. The WT strain is CCY1905. Data are from two independent experiments.
- D Ten-fold serial dilutions on the indicated media are shown. Strains engineered with the indicated mutations were tested for rescue of *BIR1* deletion. *Dam1* alleles with nonphosphorylatable mutations in *Mps1* phosphosites (S218 and S221) do not rescue growth after *bir1* Δ .

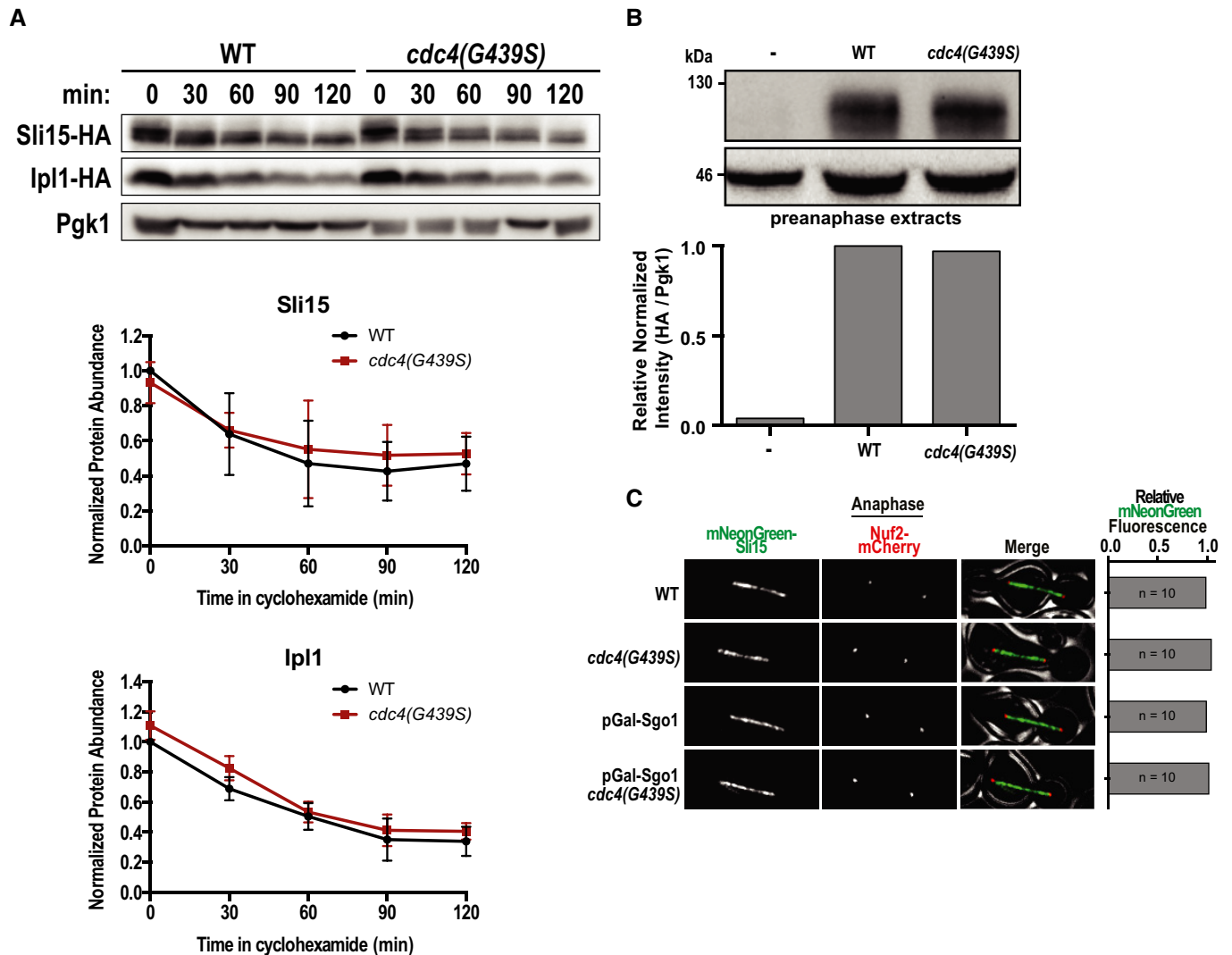


Figure EV5. Engineering and characterization of FBXW7 mutant cell lines.

- A** Strategy implemented to introduce specific point mutations in *FBXW7* in HAP1 cells. Transfected cell lines were originally screened for a silent mutation that creates an EcoR1 restriction site.
- B** Sanger sequencing confirms the presence of the G437S mutation in *FBXW7*.
- C** Cell lines mutant for *FBXW7* have an increased colony size after 12 days of growth in comparison to a cell line with wild-type *FBXW7*. Means and standard deviations are shown. Each individual value point is the size measurement of a single clone. Data are from two independent experiments. (***) $P < 0.001$; (****) $P < 0.0001$; unpaired t-test.

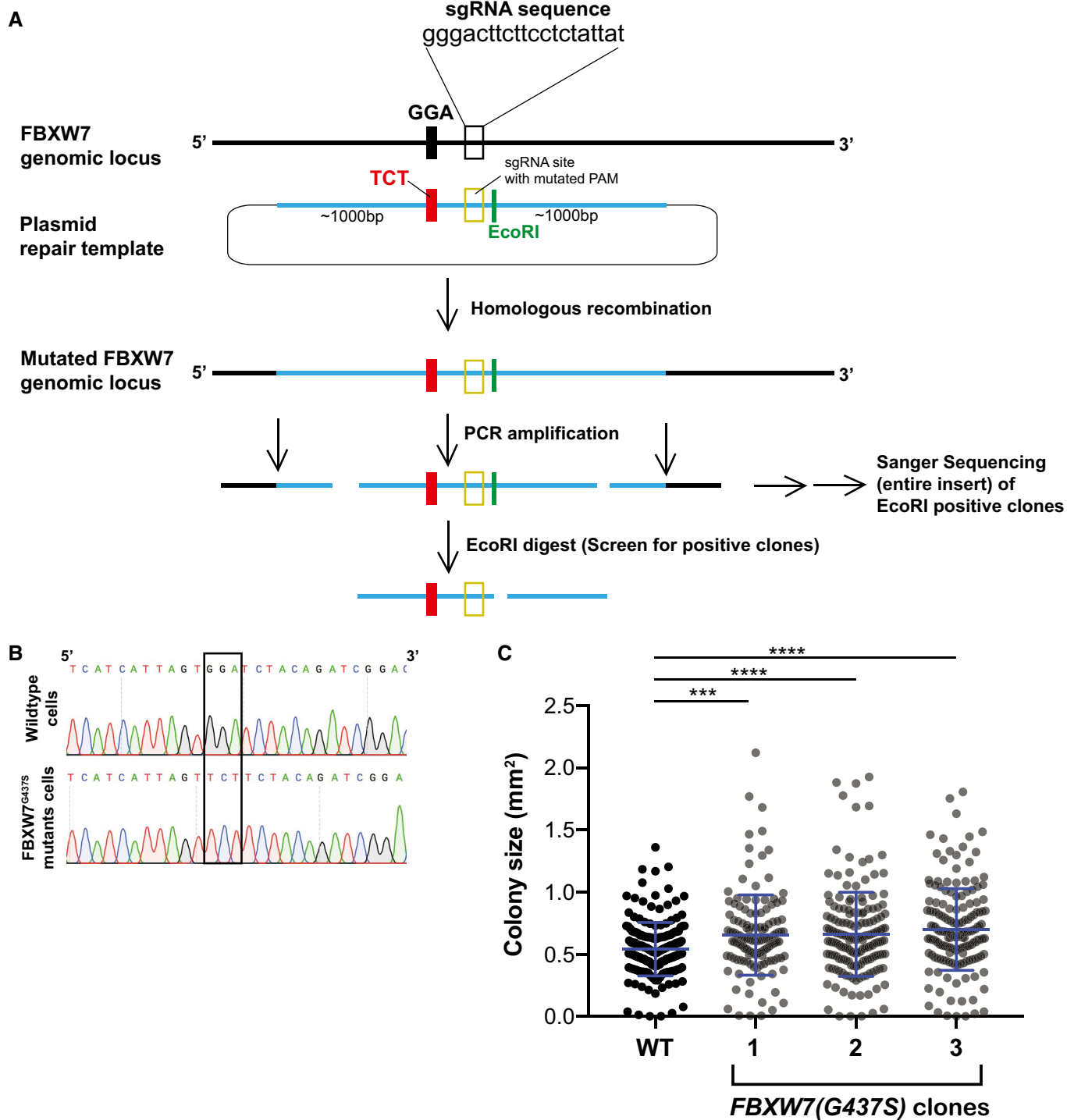


Figure EV5.